J. Fluid Mech. (2021), *vol*. 929, A13, doi:10.1017/jfm.2021.815

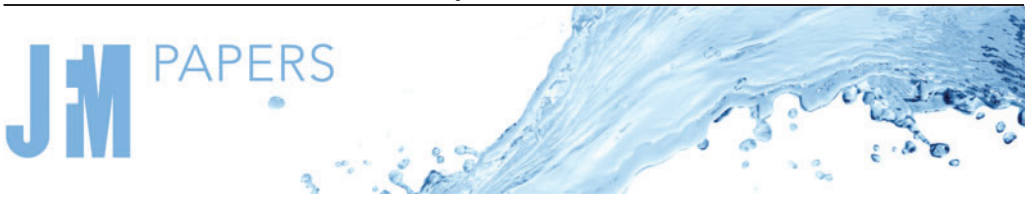

Velocity gradient statistics in turbulent shear flow: an extension of Kolmogorov's local equilibrium theory

Yukio Kaneda[1],† **and Yoshinobu Yamamoto**[2]

[1]Graduate School of Mathematics, Nagoya University, Nagoya 464-8602, Japan

[2]Department of Mechanical Engineering, University of Yamanashi, Kofu 400-8511, Japan

(Received 28 March 2021; revised 5 August 2021; accepted 14 September 2021)

This paper presents an extension of Kolmogorov's local similarity hypotheses of turbulence to include the influence of mean shear on the statistics of the fluctuating velocity in the dissipation range of turbulent shear flow. According to the extension, the moments of the fluctuating velocity gradients are determined by the local mean rate of the turbulent energy dissipation $\langle\epsilon\rangle$ per unit mass, kinematic viscosity ν and parameter $\gamma \equiv S(\nu/\langle\epsilon\rangle)^{1/2}$, provided that γ is small in an appropriate sense, where S is an appropriate norm of the local gradients of the mean flow. The statistics of the moments are nearly isotropic for sufficiently small γ, and the anisotropy of moments decreases approximately in proportion to γ. This paper also presents a report on the second-order moments of the fluctuating velocity gradients in direct numerical simulations (DNSs) of turbulent channel flow (TCF) with the friction Reynolds number Re_τ up to ≈ 8000. In the TCF, there is a range y where γ scales approximately $\propto y^{-1/2}$, and the anisotropy of the moments of the gradients decreases with y nearly in proportion to $y^{-1/2}$, where y is the distance from the wall. The theoretical conjectures proposed in the first part are in good agreement with the DNS results.

Key words: turbulence theory, turbulence simulation, turbulent boundary layers

1. Introduction

Kolmogorov introduced the idea of the local isotropy and similarity hypotheses in his celebrated work (Kolmogorov 1941), called K41. He wrote

'...we think it rather likely that in an arbitrary turbulent flow with a sufficiently large Reynolds number* $R = LU/\nu$ the hypothesis of local isotropy is realised with good

† Email address for correspondence: kaneda@math.nagoya-u.ac.jp

approximation in sufficiently small domains G of the four-dimensional space (x_1, x_2, x_3, t) not lying near the boundary of the flow or its other singularities.',

'*Here L and U denote the typical length and velocity for the flow in the whole', and ν is the kinematic viscosity, where the sentences in '...' are from Kolmogorov (1941, p. 302).

Although all is not well in the hypotheses, which ignore intermittency effects, K41 still provides reasonable approximations for low-order statistics. However, it is to be recalled that K41 assumes the influence of certain features to be negligible under the condition 'not lying near the boundary of the flow or its other singularities', while it is not *a priori* clear whether we may safely assume them to be negligible in real flows.

Among the features is the existence of mean flow gradients, which are generally neither homogeneous nor isotropic due to, for example, the existence of boundary walls and/or external forcing. In cases of wall-bounded turbulence (WBT), the mean flow gradients generally depend on the distance from the wall. One may ask how strong or weak is the influence of the mean flow gradients on the turbulence statistics? How do the statistics depend on distance from the wall in WBT? And how can one extend the idea of K41 to take into account the mean flow gradients, and so on?

K41 gives a theory for the local equilibrium statistics in the range of the scale r such that $r \ll L$. The range includes the inertial subrange (ISR) such that $\eta \ll r \ll L$, where η is the so-called Kolmogorov microscale, i.e. the characteristic length scale of small eddies where most of the kinetic energy dissipates. Regarding the ISR, studies have been made on the influence of the mean shear on the statistics such as the energy spectra and two-point moments in the range (e.g. Lumley 1967; Leslie 1973; Saddoughi & Veeravalli 1994; Yoshizawa 1998; Ishihara, Yoshida & Kaneda 2002; Yoshida, Ishihara & Kaneda 2003; Cambon & Rubinstein 2006; Tsuji & Kaneda 2012; Kaneda 2020 and references cited therein).

K41 is concerned with not only the statistics in the ISR, but also those in the dissipation range (DR) at scales $r \sim \eta$. The moments of the fluctuating velocity gradients are among the representative statistics dominated by the eddies in the DR, and have been widely studied experimentally and computationally, particularly from the energy dissipation process perspective, (e.g. Browne, Antonia & Shah 1987; Mansour, Kim & Moin 1988; Antonia, Kim & Browne 1991; George & Hussein 1991; Tsinober, Kit & Dracos 1992; Honkan & Andreopoulos 1997; Schumacher, Sreenivasan & Yeung 2003; Livescu & Madnia 2004; Bolotnov *et al.* 2010; Folz & Wallace 2010; Meneveau 2011; Loucks & Wallace 2012; Vreman & Kuerten 2014; Pumir, Xu & Siggia 2016; Pumir 2017; Tardu 2017; Lee & Moser 2019, among many others).

Studies so far made suggest that, unless the mean shear is too strong or in case of WBT the domain is too close to wall, the anisotropy of the statistics of the fluctuating velocity gradients is not very strong. However, the quantitative understanding of the influence of the mean shear on the statistics or in the cases of WBT, the understanding of the dependence of the statistics on the distance from the wall, is still challenging.

(Note: we cited here references only from the view point of the mean shear effects on the ISR spectra (correlations) and on the velocity gradient statistics. This does not imply that research on mean shear effects has been limited to those from this view point. In fact, there is a large domain of homogeneous anisotropic shear flow studies, as seen for example in the textbook by Sagaut & Cambon (2018) on anisotropic homogeneous turbulence, and references cited therein.)

The primary objective of this study is to promote our understanding of the statistics in the DR of turbulent shear flow of incompressible fluid. We pay a particular attention to

the moments of fluctuating velocity gradients. In § 2, we propose an extension of the K41 theory to take into account the influence of the mean shear on the statistics in the DR. The extension is based on the idea of the linear response theory (LRT) of turbulence (Kaneda 2020). As seen in § 2.2, the extended theory is applicable to the moments of fluctuating velocity gradients. When applied to the inertial sublayer of WBT, it gives quantitative predictions of the dependence of the moments on the distance from the wall. In § 2.3, we analyse the second-order moments C_{ijkj} that make up the so-called energy dissipation rate tensor (ϵ_{ij}), where $C_{ijmn} \equiv \langle g_{ij} g_{mn} \rangle$, g_{ij} are the fluctuating velocity gradients (see (2.21)), $\epsilon_{ij}/(2\nu) \equiv \langle g_{i1} g_{j1} \rangle + \langle g_{i2} g_{j2} \rangle + \langle g_{i3} g_{j3} \rangle$, and ν is the kinematic viscosity. The brackets $\langle \ldots \rangle$ denote an appropriate average.

In § 3, we present a report on the statistics of C_{ijkj} by a series of high-resolution direct numerical simulations (DNSs) of turbulent channel flow (TCF) of incompressible fluid with the friction Reynolds number Re_τ up to approximately 8000. The present study is the first use of the data of this high-resolution DNS series. The data supporting the findings of this study are available at http://www.me.yamanashi.ac.jp/lab/yamamoto/DNS2.html. To our knowledge, the present study is the first to present the y-dependence of the entire set of the moments C_{ijkj} for any i, j, k with $i, j, k = 1, 2, 3$ (except those that must be zero under a certain geometrical symmetry) in TCF with Re_τ as high as approximately 8000. The set allows us to know the relative magnitude of moments for different i, j, k and is expected to help develop models of the turbulent energy dissipation process in turbulent shear flows (TSFs). Moreover, the set can be used to assess theories. In fact, theoretical conjectures proposed in § 2 are compared with the DNS statistics in § 3.

2. An extension of K41 to TSF

In this study, we consider the statistics at small scales in statistically stationary TSF of incompressible fluid obeying the Navier–Stokes equation

$$\frac{\partial}{\partial t}\tilde{\boldsymbol{u}} = -(\tilde{\boldsymbol{u}} \cdot \boldsymbol{\nabla})\tilde{\boldsymbol{u}} - \frac{1}{\rho}\boldsymbol{\nabla}\tilde{p} + \nu\nabla^2\tilde{\boldsymbol{u}}, \tag{2.1}$$

where $\tilde{\boldsymbol{u}} = \tilde{\boldsymbol{u}}(\boldsymbol{x}, t)$ and $\tilde{p} = \tilde{p}(\boldsymbol{x}, t)$ are the fluid velocity and pressure, respectively, at position $\boldsymbol{x}$ and time t, and ρ is the fluid density that is constant in space and time. Particular attention is paid to the second-order moments of the fluctuating velocity gradients.

In the formulation of the K41 theory, Kolmogorov (1941) used a coordinate frame, $\mathcal{F}$, whose origin moves with the velocity at time t_0 of a fluid particle. Let $\tilde{\boldsymbol{u}}_0 \equiv \tilde{\boldsymbol{u}}(\boldsymbol{x}_0, t_0)$ be the corresponding velocity of the fluid particle, and $\boldsymbol{r}$ and $\tilde{\boldsymbol{v}}$ be the position and velocity vectors in the frame $\mathcal{F}$ such that

$$\boldsymbol{r} \equiv \boldsymbol{x} - \boldsymbol{r}_0, \quad \boldsymbol{r}_0 \equiv \boldsymbol{x}_0 + s\tilde{\boldsymbol{u}}_0, \quad s \equiv t - t_0, \tag{2.2a–c}$$

$$\tilde{\boldsymbol{v}} \equiv \tilde{\boldsymbol{v}}(\boldsymbol{r}, s) \equiv \tilde{\boldsymbol{u}}(\boldsymbol{r} + \boldsymbol{r}_0, s + t_0) - \tilde{\boldsymbol{u}}_0. \tag{2.3}$$

Kolmogorov considered a $3n$-dimensional distribution law of probabilities F_n for the quantities $\tilde{\boldsymbol{v}}^{(k)} \equiv \tilde{\boldsymbol{v}}(\boldsymbol{r}^{(k)}, s^{(k)})$ $(k = 1, 2, \ldots, n)$, where $(\boldsymbol{r}^{(k)} + \boldsymbol{r}_0, s^{(k)} + t_0)$ are points in the four-dimensional space $(\boldsymbol{x}, t)$ in the domain G under consideration. After setting up the idea of local homogeneity and isotropy in the domain G, he introduced two hypotheses of similarity, the first of which is the following:

'The first hypothesis of similarity.

For the locally isotropic turbulence the distributions F_n are uniquely determined by the quantities ν and $\langle \epsilon \rangle$.' (Kolmogorov 1941, p. 304)

Here, $\langle\epsilon\rangle$ is the mean rate of the energy dissipation ϵ per unit mass. (The symbol $\bar{\epsilon}$ instead of $\langle\epsilon\rangle$ was used in K41.)

2.1. *An extension of K41 by the idea of LRT*

In the study of TSF, it is common practice to decompose the filed $\tilde{\boldsymbol{u}}$ into a mean $\boldsymbol{U}$ and fluctuating part $\boldsymbol{u}$ such that $\tilde{\boldsymbol{u}} = \boldsymbol{U} + \boldsymbol{u}$. Corresponding to this decomposition, $\tilde{\boldsymbol{v}}$ defined by (2.3) can be decomposed as

$$\tilde{\boldsymbol{v}} = \tilde{\boldsymbol{v}}(\boldsymbol{r}, s) = \boldsymbol{V}(\boldsymbol{r}, s) + \boldsymbol{v}(\boldsymbol{r}, s), \tag{2.4}$$

where

$$\boldsymbol{V} = \boldsymbol{V}(\boldsymbol{r}, s) = \boldsymbol{U}(\boldsymbol{r} + \boldsymbol{r}_0, s + t_0) - \boldsymbol{U}(\boldsymbol{x}_0, t_0), \tag{2.5}$$

$$\boldsymbol{v} = \boldsymbol{v}(\boldsymbol{r}, s) = \boldsymbol{u}(\boldsymbol{r} + \boldsymbol{r}_0, s + t_0) - \boldsymbol{u}(\boldsymbol{x}_0, t_0). \tag{2.6}$$

In the frame $\mathcal{F}$, we have

$$\frac{\partial}{\partial s}\boldsymbol{v} = -(\boldsymbol{V}\cdot\boldsymbol{\nabla})\boldsymbol{v} - (\boldsymbol{v}\cdot\boldsymbol{\nabla})\boldsymbol{V} - (\boldsymbol{v}\cdot\boldsymbol{\nabla})\boldsymbol{v} + \langle(\boldsymbol{v}\cdot\boldsymbol{\nabla})\boldsymbol{v}\rangle - \frac{1}{\rho}\boldsymbol{\nabla}p + \nu\nabla^2\boldsymbol{v} - \boldsymbol{R}, \tag{2.7}$$

for the fluctuating field $(\boldsymbol{v}, p)$, where $p \equiv \tilde{p} - \langle p\rangle$, $\boldsymbol{R} \equiv (\boldsymbol{u}(\boldsymbol{x}_0, t_0)\cdot\boldsymbol{\nabla})\boldsymbol{V}$, $\boldsymbol{\nabla} = (\partial/\partial x_1, \partial/\partial x_2, \partial/\partial x_3) = (\partial/\partial r_1, \partial/\partial r_2, \partial/\partial r_3)$, and a_i is the ith Cartesian component of vector $\boldsymbol{a}$.

In this subsection, we propose an extension of K41 on the basis of the application of the idea of the LRT. The application is based on rough estimates of terms in (2.7) for eddies of scales $\sim \eta$. As seen below, the estimates can be obtained in a simple way similar to those presented in studies including e.g. Kaneda & Yoshida (2004), Kaneda (2020), which give estimates for eddies of scales $\ll L_U$, in the context of the applications of the idea of LRT to turbulent flows, where L_U is the characteristic length scale of $\boldsymbol{U}$.

Since at time $t = t_0$, i.e. $s = 0$, $\boldsymbol{V}$ can be expanded for $r \equiv |\boldsymbol{r}| \ll L_U$ as

$$\boldsymbol{V} = \boldsymbol{U}(\boldsymbol{r} + \boldsymbol{x}_0, t_0) - \boldsymbol{U}(\boldsymbol{x}_0, t_0) = \frac{\partial \boldsymbol{U}}{\partial x_\alpha} r_\alpha + \cdots, \tag{2.8}$$

we have at the time instant $s = 0$,

$$(\boldsymbol{V}\cdot\boldsymbol{\nabla})\boldsymbol{v} + (\boldsymbol{v}\cdot\boldsymbol{\nabla})\boldsymbol{V} = \left(\frac{\partial U_\alpha}{\partial x_\beta} r_\beta\right)\frac{\partial \boldsymbol{v}}{\partial r_\alpha} + v_\alpha \frac{\partial \boldsymbol{U}}{\partial x_\alpha} + \cdots, \tag{2.9}$$

for $r \ll L_U$, where the summation convention is used for repeated Greek indices, $\partial U_i/\partial x_j$ are the mean flow gradients at $\boldsymbol{x} = \boldsymbol{x}_0$, i.e. they are $\partial U_i/\partial x_j|_{\boldsymbol{x}=\boldsymbol{x}_0}$ and we omit the symbol '$|_{\boldsymbol{x}=\boldsymbol{x}_0}$' for ease of writing, and we have used $\partial u_i/\partial x_j = \partial v_i/\partial r_j$. We assume time dependence of $\boldsymbol{U}$ to be negligible in the following. We also assume that L_U is so large that the gradients of $\boldsymbol{R}$ in (2.7) are sufficiently small, i.e. $\boldsymbol{R}$ is almost constant in the domain $r \ll L_U$, and therefore $\boldsymbol{R}$ is negligible in considering the small-scale statistics, such as those of velocity differences between two points, in the domain.

Rough order estimates of the first three terms on the right-hand side of (2.7) and the terms in (2.9) for $r \sim \eta$ can be obtained by putting $\boldsymbol{v} \sim v_\eta$, $\boldsymbol{\nabla}\boldsymbol{v} \sim v_\eta/\eta$ and $\nabla^2\boldsymbol{v} \sim v_\eta/\eta^2$, where η is the Kolmogorov length scale given by $\eta = (\nu^3/\langle\epsilon\rangle)^{1/4}$, v_η is the characteristic velocity scale of eddies of scales $\sim \eta$ and given by $v_\eta \sim (\langle\epsilon\rangle\,\nu)^{1/4}$, ϵ is the local rate of the energy dissipation per unit mass that is due to solely the fluctuating part $\boldsymbol{u}$ and defined independently of the mean flow $\boldsymbol{U}$ (ϵ is simply called the energy dissipation rate

in the following) and the symbol '$\sim$' denotes equality in the order of magnitude. Then, we obtain

$$\left(\frac{\partial U_\alpha}{\partial x_\beta} r_\beta\right) \frac{\partial \boldsymbol{v}}{\partial r_\alpha} + v_\alpha \frac{\partial \boldsymbol{U}}{\partial x_\alpha} \sim S v_\eta = S(\langle\epsilon\rangle\, \nu)^{1/4}, \tag{2.10}$$

$$(\boldsymbol{v} \cdot \boldsymbol{\nabla})\boldsymbol{v} \sim \frac{v_\eta^2}{\eta} = \left(\frac{\langle\epsilon\rangle^3}{\nu}\right)^{1/4}, \tag{2.11}$$

and

$$\nu \nabla^2 \boldsymbol{v} \sim \frac{\nu v_\eta}{\eta^2} = \left(\frac{\langle\epsilon\rangle^3}{\nu}\right)^{1/4}, \tag{2.12}$$

where S is an appropriate norm of the tensor $(\partial U_i/\partial x_j)$ such as $[(\partial U_\alpha/\partial x_\beta)(\partial U_\alpha/\partial x_\beta)]^{1/2}$, and it is assumed that $\eta \ll L_U$ and L.

Equations (2.10)–(2.12) give

$$(\boldsymbol{V} \cdot \boldsymbol{\nabla})\boldsymbol{v} + (\boldsymbol{v} \cdot \boldsymbol{\nabla})\boldsymbol{V} \sim \gamma[(\boldsymbol{v} \cdot \boldsymbol{\nabla})\boldsymbol{v}] \sim \gamma[\nu \nabla^2 \boldsymbol{v}], \tag{2.13}$$

where γ is the ratio of the time scale $\tau_\eta \equiv \eta/v_\eta$ of small eddies of size $\sim \eta$ to the time scale $\tau_S \equiv 1/S$ associated with the mean shear,

$$\gamma \equiv \frac{\eta/v_\eta}{1/S} = S\frac{\eta}{v_\eta} = \frac{S(\langle\epsilon\rangle\, \nu)^{1/4}}{(\langle\epsilon\rangle^3/\nu)^{1/4}} = S\left(\frac{\nu}{\langle\epsilon\rangle}\right)^{1/2}. \tag{2.14}$$

Equation (2.13) implies that γ may be interpreted not only as the time ratio τ_η/τ_S, but also as the time ratio τ_N/τ_S for eddies of scales $\sim \eta$, where τ_N is the characteristic time scale associated with the convection term $(\boldsymbol{v} \cdot \boldsymbol{\nabla})\boldsymbol{v}$.

Equation (2.13) also implies that if

$$\gamma \equiv S\left(\frac{\nu}{\langle\epsilon\rangle}\right)^{1/2} \ll 1, \tag{2.15}$$

then the magnitude of the first two terms on the right-hand side of (2.7), i.e. the terms representing the direct coupling between $\boldsymbol{v}$ and the mean flow $\boldsymbol{V}$, is negligibly small compared with that of the nonlinear coupling term $(\boldsymbol{v} \cdot \boldsymbol{\nabla})\boldsymbol{v}$ and the viscous term $\nu \nabla^2 \boldsymbol{v}$. This suggests that, if $\gamma \ll 1$, then the influence of the two terms on the distribution law of probabilities F_n for $r \sim \eta$, is negligibly small compared with those of $(\boldsymbol{v} \cdot \boldsymbol{\nabla})\boldsymbol{v}$ and $\nu \nabla^2 \boldsymbol{v}$. If the two terms and $\boldsymbol{R}$ can be ignored, then the equation of motion (2.7) is compatible with isotropy, i.e. invariant to arbitrary rotation of the coordinate system.

(Note: by comparing the characteristic inertial transfer time scale and the time scale ($\sim 1/S$) associated with the mean shear in the wavenumber range $\sim k$, and by using the ISR energy spectrum given by K41, Corrsin (1958) argued that

$$k^{2/3} \gg \langle\epsilon\rangle^{-1/3} S \tag{2.16}$$

need be satisfied for the local isotropy of the statistics in the wavenumber range $\sim k$ in the ISR of TSF. Here, we are ignoring constants of order unity. If we put $k \sim 1/\eta$, then (2.16) gives (2.15). In terms of length scales, the inequalities (2.15) and (2.16) are respectively equivalent to $\eta/L_C \ll 1$ and $\ell/L_C \ll 1$ with $\ell \sim 1/k$, where L_C is Corrsin's length scale given by $L_C = (\langle\epsilon\rangle/S^3)^{1/2}$.)

These observations suggest to us to exploit the idea of LRT of turbulence. LRT is based on the assumption of the existence of a certain kind of equilibrium state under certain conditions. Suppose that a disturbance, say X, is added to a system that is in an equilibrium state in the absence of X. Then, in response to this disturbance, the statistical average $\langle B\rangle$ of observable B changes from $\langle B\rangle_e$ to

$$\langle B\rangle = \langle B\rangle_e + \Delta\langle B\rangle\,, \tag{2.17}$$

where $\langle B\rangle_e$ is the average in the equilibrium state in the absence of X, and $\Delta\langle B\rangle$ denotes the change owing to X. In LRT, it is assumed that if X is appropriately small, then $\Delta\langle B\rangle$ can be approximated to be the first order in X, i.e.

$$\Delta\langle B\rangle = \Delta_1\langle B\rangle + \cdots\,, \tag{2.18}$$

where $\Delta_1\langle B\rangle$ denotes a first-order term in X and '$\cdots$' denotes higher-order terms in X; $\Delta_1\langle B\rangle$ can be written as

$$\Delta_1\langle B\rangle = cX, \tag{2.19}$$

in which X is to be understood as a measure representing the disturbance in an appropriate sense, and c is a coefficient determined by the nature of the equilibrium state, independently of X. If the disturbance consists of more than one type of disturbance, $X_1, X_2, \ldots$, (2.19) is to be understood as

$$\Delta_1\langle B\rangle = c_1X_1 + c_2X_2 + \cdots\,, \tag{2.20}$$

where c_1 and c_2 are constants. Readers may refer to Kaneda (2020) for some details on the idea of LRT applied to turbulent flows.

In accordance with K41, we assume here that, in the limit of small γ, the turbulence domain G under consideration is in a locally isotropic equilibrium state satisfying the first hypothesis of similarity, and we apply the idea of LRT to estimate the influence of small but finite γ on the statistics at small scales $\sim\eta$ in TSF. Let B be an observable whose average is dominated by the statistics at scales $r\sim\eta$. We assume the following three hypotheses.

(i) The first hypothesis of similarity for TSF.
In the limit $\gamma\to 0$, the statistics of B are locally isotropic, and the average $\langle B\rangle$ is uniquely determined by ν and the local quantity $\langle\epsilon\rangle$ independently of the mean flow gradients $\partial U_i/\partial x_j$.

Regarding the effect of small but finite γ:

(ii) The second hypothesis of similarity for TSF.
For sufficiently small but finite γ, the change $\Delta\langle B\rangle$ of $\langle B\rangle$ owing to the mean shear can be approximated to be linear in γ, i.e. $\Delta\langle B\rangle\approx\Delta_1\langle B\rangle$, where $\Delta_1\langle B\rangle = c\gamma$, in which the coefficient c is independent of γ.

(iii) The third hypothesis of similarity for TSF.
The coefficient c is uniquely determined by the locally isotropic equilibrium state in the absence of mean shear, so that it is uniquely determined by ν and the local quantity $\langle\epsilon\rangle$.

In the context considering the dependence of statistics on γ at small γ, the symbol '$\approx$' denotes equality in the sense of neglecting terms of order higher in γ than that (those) of the retained term(s).

The local equilibrium state assumed in K41 and the first hypothesis of similarity for TSF can in general be disturbed not only by the mean shear, but also by other effects such as the anisotropy in energy-containing eddies and inhomogeneity of the pressure field due to the existence of the boundary wall. Regarding the influence of anisotropy in energy-containing eddies, see the discussions in § 4.1. The main interest of this study is the influence of the mean shear, and it is assumed that the other effects, if there are any, on the statistics at scales $\sim \eta$ are insignificant or at most of an order of magnitude similar to that of the effect of the mean shear. LRT suggests that if such other effects are not negligible, then one may add their influence as in (2.20), provided that they are small in an appropriate sense.

2.2. *Application to the statistics of velocity gradients*

Let g_{ij} be the gradient of the fluctuating velocity field given by

$$g_{ij} \equiv g_{ij}(\boldsymbol{x}, t) \equiv \frac{\partial u_i}{\partial x_j} = \frac{\partial v_i}{\partial r_j}. \tag{2.21}$$

It is natural to assume that the pth-order moments $\langle g_{ij}g_{mn}\cdots\rangle$ are dominated by the statistics of small eddies in the energy dissipation scale range. The application of the first hypothesis of similarity for TSF to $B = g_{ij}g_{mn}\cdots$ then gives the following for pth-order moments

$$\langle g_{ij}g_{mn}\cdots\rangle \to \langle g_{ij}g_{mn}\cdots\rangle_e = f^{(p)}_{ijmn\ldots}(\nu, \langle\epsilon\rangle), \tag{2.22}$$

in the limit of sufficiently small γ, where $f^{(p)}_{ijmn\ldots}$ is an appropriate isotropic tensor depending only on ν and local average $\langle\epsilon\rangle$ at position $\boldsymbol{x}$. A dimensional consideration gives

$$\langle g_{ij}g_{mn}\cdots\rangle_e = \left(\frac{\langle\epsilon\rangle}{\nu}\right)^{p/2} C^{(p)}_{e,ijmn\ldots}, \tag{2.23}$$

where $C^{(p)}_{e,ijmn\ldots}$ are dimensionless $2p$th-order isotropic tensors. If γ is small but finite, then $\langle g_{ij}g_{mn}\cdots\rangle$ generally change from $\langle g_{ij}g_{mn}\cdots\rangle_e$ to

$$\langle g_{ij}g_{mn}\cdots\rangle = \langle g_{ij}g_{mn}\cdots\rangle_e + \Delta\langle g_{ij}g_{mn}\cdots\rangle, \tag{2.24}$$

where $\Delta\langle g_{ij}g_{mn}\cdots\rangle$ are the changes due to the disturbance by the small but finite mean shear, represented by γ. The second hypothesis of similarity for TSF implies that $\Delta\langle g_{ij}g_{mn}\cdots\rangle$ can be approximated to be linear in γ, so that

$$\Delta\langle g_{ij}g_{mn}\cdots\rangle \approx \Delta_1\langle g_{ij}g_{mn}\cdots\rangle = c^{(p)}_{1,ijmn\ldots}\gamma, \tag{2.25}$$

in which the coefficients $c^{(p)}_{1,ijmn\ldots}$ are independent of γ. The third hypothesis of similarity for TSF implies that the coefficients $c_{1,ijmn\ldots}$ depend only on $\langle\epsilon\rangle$ and ν. A dimensional consideration then gives

$$\Delta_1\langle g_{ij}g_{mn}\cdots\rangle = \gamma\left(\frac{\langle\epsilon\rangle}{\nu}\right)^{p/2} C^{(p)}_{1,ijmn\ldots}, \tag{2.26}$$

where $C^{(p)}_{1,ijmn\ldots}$ are dimensionless constants.

From (2.23)–(2.26), we have for $p = 2$,

$$\left\langle g_{ij}g_{mn}\right\rangle \approx \left\langle g_{ij}g_{mn}\right\rangle_e + \Delta_1 \left\langle g_{ij}g_{mn}\right\rangle = \frac{\langle\epsilon\rangle}{\nu}\left(C_{e,ijmn} + \gamma C_{1,ijmn}\right), \tag{2.27}$$

where $C_{e,ijmn}$ and $C_{1,ijmn}$ are dimensionless constants independent of ν, $\langle\epsilon\rangle$ and S, and superscript '(2)' is omitted for simplicity. The second hypothesis of similarity for TSF implies that $C^{(p)}_{1,ijmn\ldots}$ are dimensionless constant tensors that are independent of the norm S, but it does not exclude the possibility of the dependence of $C_{1,ijmn}$ on components $(\partial U_i/\partial x_j)/S$. (See discussions in § 4.2.)

Since $C_{e,ijmn}$ is a fourth-order isotropic tensor, it may be written without loss of generality as

$$C_{e,ijmn} = a\delta_{ij}\delta_{mn} + b\delta_{im}\delta_{jn} + c\delta_{in}\delta_{jm}, \tag{2.28}$$

where a, b and c are dimensionless constants that are independent of $\langle\epsilon\rangle$ and ν. (This c is to be not confused with c in the other contexts such as in (2.19).) Since $g_{\alpha\alpha} = 0$ due to the incompressibility condition, we have $C_{e,\alpha\alpha mn} = 0$ for any m, n, so that

$$C_{e,\alpha\alpha mn} = 3a\delta_{mn} + b\delta_{mn} + c\delta_{mn} = 0, \tag{2.29}$$

i.e.

$$3a + b + c = 0. \tag{2.30}$$

If the flow statistics are homogeneous in two Cartesian directions, say in the x_1- and x_3-directions, then

$$\begin{aligned}\langle g_{13}g_{31}\rangle - \langle g_{11}g_{33}\rangle &= \left\langle \frac{\partial u_1}{\partial x_3}\frac{\partial u_3}{\partial x_1}\right\rangle - \left\langle \frac{\partial u_1}{\partial x_1}\frac{\partial u_3}{\partial x_3}\right\rangle \\ &= \frac{\partial}{\partial x_3}\left\langle u_1\frac{\partial u_3}{\partial x_1}\right\rangle - \frac{\partial}{\partial x_1}\left\langle u_1\frac{\partial u_3}{\partial x_3}\right\rangle = 0.\end{aligned} \tag{2.31}$$

Equation (2.31) implies $C_{e,1331} = C_{e,1133}$, so that we have $c = a$ from (2.28) (cf. Kida & Orszag (1990)). Then, (2.30) gives $b = -4a$, so that (2.28) can be reduced to

$$C_{e,ijmn} = a\left(\delta_{ij}\delta_{mn} - 4\delta_{im}\delta_{jn} + \delta_{in}\delta_{jm}\right). \tag{2.32}$$

Because

$$\epsilon = 2\nu s_{\alpha\beta}s_{\alpha\beta}, \tag{2.33}$$

in which $s_{ij} = (g_{ij} + g_{ji})/2$, we have $\langle\epsilon\rangle/\nu = \left\langle(g_{\alpha\beta} + g_{\beta\alpha})g_{\alpha\beta}\right\rangle$. Therefore, (2.27) yields $C_{e,\alpha\beta\alpha\beta} = 1$. Thus (2.32) gives

$$a = -\tfrac{1}{30} \tag{2.34}$$

(see § 3.1). Note that statistical homogeneity in the x_2-direction is not assumed in the derivation of (2.32), but (2.32) is still the same as the well-known expression for $\left\langle g_{ij}g_{mn}\right\rangle$ in homogeneous and isotropic turbulence (cf. e.g. Hinze 1975; Kida & Orszag 1990; Pumir 2017).

Equations (2.27), (2.32) and (2.34) give among others

$$\frac{\nu}{\langle\epsilon\rangle}\left\langle\left(\frac{\partial u_i}{\partial x_i}\right)^2\right\rangle=\frac{\nu}{\langle\epsilon\rangle}\langle g_{ii}g_{ii}\rangle\approx\frac{1}{15}+\gamma C_{1,iiii}, \tag{2.35}$$

$$\frac{\nu}{\langle\epsilon\rangle}\left\langle\left(\frac{\partial u_i}{\partial x_j}\right)^2\right\rangle=\frac{\nu}{\langle\epsilon\rangle}\langle g_{ij}g_{ij}\rangle\approx\frac{2}{15}+\gamma C_{1,ijij}, \tag{2.36}$$

$$\frac{\nu}{\langle\epsilon\rangle}\left\langle\frac{\partial u_i}{\partial x_j}\frac{\partial u_k}{\partial x_j}\right\rangle=\frac{\nu}{\langle\epsilon\rangle}\langle g_{ij}g_{kj}\rangle\approx\gamma C_{1,ijkj}, \tag{2.37}$$

and

$$\frac{\left\langle(\partial u_i/\partial x_j)^2\right\rangle}{\left\langle(\partial u_i/\partial x_i)^2\right\rangle}=\frac{\langle g_{ij}g_{ij}\rangle}{\langle g_{ii}g_{ii}\rangle}\approx 2+\gamma(15C_{1,ijij}-30C_{1,iiii}), \tag{2.38}$$

where $i\neq j$, $i\neq k$, no summation is taken over repeated italic indices and in (2.37) we have used $C_{e,ijkj}=0$ because of (2.32).

Equations (2.27), (2.32) and (2.34) also give

$$\frac{\nu}{\langle\epsilon\rangle}\left\langle\frac{\partial u_i}{\partial x_\alpha}\frac{\partial u_j}{\partial x_\alpha}\right\rangle=\frac{\nu}{\langle\epsilon\rangle}\langle g_{i\alpha}g_{j\alpha}\rangle=\frac{\epsilon_{ij}}{2\langle\epsilon\rangle}\approx\frac{1}{3}\delta_{ij}+\gamma C_{1,i\alpha j\alpha}, \tag{2.39}$$

where ϵ_{ij} is defined by $\epsilon_{ij}\equiv 2\nu\langle g_{i\alpha}g_{j\alpha}\rangle$, and we used $C_{e,i\alpha j\alpha}=(1/3)\delta_{ij}$.

Constants $1/15$, $2/15$, 2 and $1/3$ on the right-hand side of (2.35), (2.36), (2.38) and (2.39) are derived from the isotropic tensor $C_{e,ijmn}$ given by (2.32) with (2.34), i.e. they agree with the results obtained by ignoring the anisotropy of statistics.

2.3. *Statistics in the inertial sublayer of the turbulent boundary layer*

It is known that in a turbulent boundary layer with mean flow $\boldsymbol{U}=(U_1,U_2,U_3)\equiv\langle\tilde{\boldsymbol{u}}\rangle=(U(y),0,0)$ at sufficiently large Re_τ and y^+, there is flow region called the inertial sublayer in which the mean flow $U(y)$ is approximately given by

$$\left(\frac{\mathrm{d}U}{\mathrm{d}y}\right)^+\approx\frac{1}{\kappa y^+}, \tag{2.40}$$

where the coefficient κ is a dimensionless constant known as the constant of von Kármán, y is the distance from the wall, symbol $^+$ denotes the normalisation by the wall-friction velocity given by $u_\tau^2=\nu(\mathrm{d}U/\mathrm{d}y)|_{y=0}$ and the wall-friction length is defined by $\ell_\tau=\nu/u_\tau$. The friction Reynolds number Re_τ is given by $Re_\tau\equiv u_\tau\delta/\nu$, where δ is the channel half-width. In this study, we use $\boldsymbol{x}=(x_1,x_2,x_3)=(x,y,z)$, and we assume $(\mathrm{d}U/\mathrm{d}y)>0$ unless otherwise stated.

It is also known that the mean energy dissipation rate $\langle\epsilon\rangle$ in the inertial sublayer is approximately given by

$$\langle\epsilon\rangle^+\approx\frac{1}{\kappa_\epsilon y^+}, \tag{2.41}$$

where κ_ϵ is a dimensionless constant (see the discussion in § 3.2). If $-\langle u_1u_2\rangle\approx(u_\tau)^2$ and if the turbulence production rate $-\langle u_1u_2\rangle\,\mathrm{d}U/\mathrm{d}y$ is mainly balanced by the mean energy dissipation rate $\langle\epsilon\rangle$ in the inertial sublayer, then we have (2.41) with $\kappa_\epsilon=\kappa$ (see e.g. Tennekes & Lumley 1972).

In such a layer, we have

$$\gamma = S\left(\frac{\nu}{\langle\epsilon\rangle}\right)^{1/2} \approx K(y^+)^{-1/2}, \quad \left(K \equiv \frac{\kappa_\epsilon^{1/2}}{\kappa}\right), \tag{2.42}$$

and

$$\eta^+ \equiv \left[\left(\frac{\nu^3}{\langle\epsilon\rangle}\right)^{1/4}\right]^+ \approx (\kappa_\epsilon y^+)^{1/4}, \tag{2.43}$$

where $\mathrm{d}U/\mathrm{d}y$ is used as the norm S of the gradient tensor $(\mathrm{d}U_i/\mathrm{d}x_j)$ of the mean velocity.

Substitution of (2.42) into (2.35)–(2.39) gives

$$\frac{\nu}{\langle\epsilon\rangle}\left\langle\left(\frac{\partial u_i}{\partial x_i}\right)^2\right\rangle = \frac{\nu}{\langle\epsilon\rangle}\langle g_{ii}g_{ii}\rangle \approx \frac{1}{15} + C_{1,iiii}\times K\times (y^+)^{-1/2}, \tag{2.44}$$

$$\frac{\nu}{\langle\epsilon\rangle}\left\langle\left(\frac{\partial u_i}{\partial x_j}\right)^2\right\rangle = \frac{\nu}{\langle\epsilon\rangle}\langle g_{ij}g_{ij}\rangle \approx \frac{2}{15} + C_{1,ijij}\times K\times (y^+)^{-1/2}, \tag{2.45}$$

$$\frac{\nu}{\langle\epsilon\rangle}\left\langle\frac{\partial u_i}{\partial x_j}\frac{\partial u_k}{\partial x_j}\right\rangle = \frac{\nu}{\langle\epsilon\rangle}\langle g_{ij}g_{kj}\rangle \approx C_{1,ijkj}\times K\times (y^+)^{-1/2}, \tag{2.46}$$

$$\frac{\left\langle(\partial u_i/\partial x_j)^2\right\rangle}{\left\langle(\partial u_i/\partial x_i)^2\right\rangle} = \frac{\langle g_{ij}g_{ij}\rangle}{\langle g_{ii}g_{ii}\rangle} \approx 2 + (15C_{1,ijij} - 30C_{1,iiii})\times K\times (y^+)^{-1/2}, \tag{2.47}$$

and

$$\frac{\epsilon_{ij}}{2\langle\epsilon\rangle} \approx \frac{1}{3}\delta_{ij} + C_{1,i\alpha j\alpha}\times K\times (y^+)^{-1/2}, \tag{2.48}$$

to the leading order of small $1/y^+$; higher-order terms in $1/y^+$ are omitted in (2.44)–(2.48).

3. Statistics in DNS of turbulent channel flow

This section presents the statistics in DNS of fully developed TCF and compares the statistics with the theoretical conjectures discussed in the previous section.

3.1. *Data resources*

Our statistical analysis was based on a database, which we call DB-TCF, produced from a series of DNSs of TCF with friction Reynolds numbers Re_τ up to approximately 8000. The DNSs use a Fourier-spectral method in the wall-parallel, i.e. x- and z-directions, and a second-order accurate finite-difference method in the wall-normal, i.e. y direction. Alias errors associated with the pseudo-spectral method are removed using the 3/2 rule. This implies that $(N_xN_z)\times(3/2)^2$ collocation points are used to evaluate the nonlinear convolution terms at each y in the DNSs. Readers may refer to Yamamoto & Kunugi (2011, 2016) for the details of the numerical schemes used in the DNSs.

Some of the key DNS parameters are listed in table 1. The initial conditions of R8000 were given by a field generated in a previous DNS (Yamamoto & Tsuji 2018) at $Re_\tau \approx$ 8000, which used a spatial-resolution and discretisation scheme differing from those of R8000. The statistics of R8000 presented below were obtained from a time interval after a certain initial transient period. In practice, we put the initial transient period of R8000

Run	Re_τ	U_b^+	L_x/δ	L_z/δ	N_x	N_y	N_z	$(\Delta x)^+$	$(\Delta y)^+$	$(\Delta z)^+$	T^+/Re_τ	N_t
R500	500	18.1	16.0	6.4	500	384	384	16.0	0.4-5.3	8.3	13.1	60
R1000	1000	20.0	16.0	6.4	1000	512	768	16.0	0.6-8.0	8.3	12.0	55
R2000	2000	21.7	16.0	6.4	2000	1024	1536	16.0	0.6-8.0	8.3	10.0	92
R4000	3996	23.4	16.0	6.4	4000	2048	3072	16.0	0.6-8.0	8.3	14.0	—
R8000	7987	25.0	16.0	6.4	6912	4096	5760	18.5	0.6-8.0	8.9	7.5	76
R1000L	1000	20.0	16.0	6.4	864	512	720	18.5	0.6-8.0	8.9	13.0	—
R1000H	1000	20.0	16.0	6.4	2048	512	1536	7.8	0.6-8.0	4.2	13.0	—

Table 1. DNS parameters. Here, U_b is the bulk velocity, L_x and L_z are respectively the fundamental periodicity length in the x- and z-directions, N_x (Δx), N_y (Δy) and N_z (Δz) are respectively the grid numbers (width) in the x-,y- and z-directions, T is the simulation time interval after the initial transient period and N_t is the number of flow fields used to compute the second-order moments $\langle g_{ij}g_{mn}\rangle$ of the fluctuating velocity gradients.

to be $3Re_\tau$ in wall units. The length of the simulation time interval $7.5Re_\tau$ in wall units as shown in table 1 is approximately equal to 11.7 T_w, where T_w is the wash-out time given by $T_w \equiv L_x/U_c$, in which U_c is the mean centre-line velocity. The statistics of the other runs were also obtained from a time interval (denoted by T in table 1) after a certain initial transient period, which we put to at least $3Re_\tau$ in wall units. It was confirmed that the total shear stress fits the linear profile in all the runs within an error of at most 0.05 in wall units as in previous DNSs (Yamamoto & Tsuji 2018). Furthermore, the mean spanwise velocity component normalised by the mean streamwise velocity component is less than 0.07 % at any y in all the runs.

The second-order moments $\langle g_{ij}g_{mn}\rangle$ of the fluctuating velocity gradients were computed by using several velocity fields stored in the DB-TCF database, and by taking the averages over the homogeneous directions (i.e. the x- and z-directions) and time. The number of fields is denoted as N_t in table 1. With regards to R4000, such a field is not available in the database, so that no statistics of $\langle g_{ij}g_{mn}\rangle$ by R4000 are presented below.

Let $\epsilon_g \equiv \nu g_{\alpha\beta}g_{\alpha\beta}$. In homogeneous turbulence, we have $\langle\epsilon_g\rangle = \langle\epsilon\rangle$. It is easy to reformulate or re-interpret the theory presented in § 2 using ϵ_g instead of ϵ. Then, we only need to change appropriately ϵ to ϵ_g in and after the first hypothesis of similarity for TSF in § 2. Regarding (2.33), it is to be replaced by $\epsilon_g = \nu g_{\alpha\beta}g_{\alpha\beta}$, but (2.27), (2.32) and (2.34) with ϵ replaced by ϵ_g remain valid.

In the analysis of the energy budget in WBT, ϵ_g plays key roles (see Appendix A), and it is convenient to use ϵ_g rather than ϵ as a measure representing the energy dissipation rate. In fact, ϵ_g has been commonly used in research investigating the WBT budget. The use of ϵ_g makes it easier for us to compare the DNS results in this study with the reported findings, as shown in figures 2(*a*) and 2(*b*) below. In the following in this section and in Appendix A, we therefore use ϵ_g instead of ϵ as the measure representing the energy dissipation rate, and we omit the subscript g, i.e. we use the symbol ϵ_g to mean $\nu g_{\alpha\beta}g_{\alpha\beta}$, unless otherwise stated. It is known that the difference between $\langle\epsilon\rangle$ and $\langle\epsilon_g\rangle$ is small in WBT for a wide range of Reynolds numbers, at least outside near the wall region (see e.g. Antonia *et al.* 1991; Bradshaw & Perot 1993; Folz & Wallace 2010; Tardu 2017). This is also confirmed in our DNS results as shown in figure 1. It is unlikely that the difference would significantly affect the discussions in this paper.

R1000L and R1000H were performed to check the possible influence of spatial resolution on the statistics at the energy DR scales. Although the grid width Δy in the

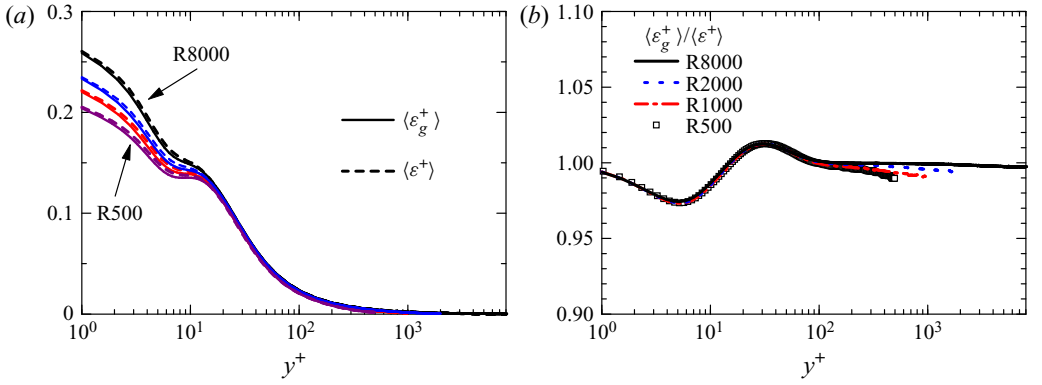

Figure 1. Comparison between $\langle \epsilon_g \rangle$ and $\langle \epsilon \rangle$. (*a*) Distributions of $\langle \epsilon_g \rangle$ and $\langle \epsilon \rangle$ and (*b*) ratio $\langle \epsilon_g \rangle / \langle \epsilon \rangle$.

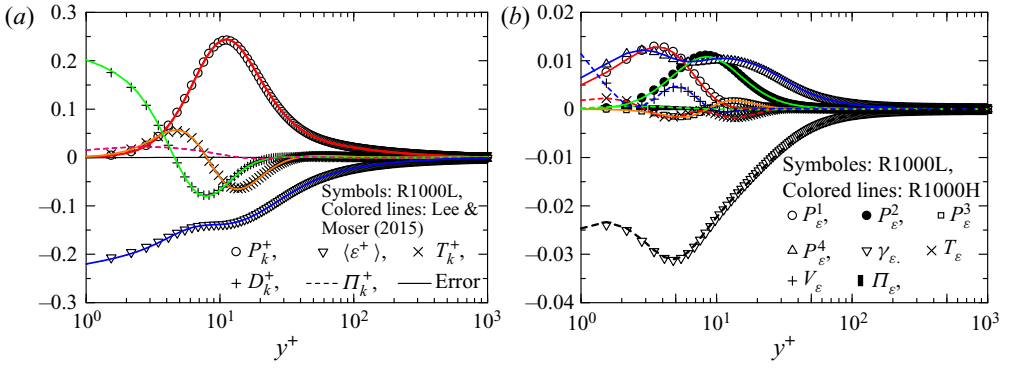

Figure 2. Grid-sensitivity analysis for R1000L, (*a*) k-budget terms in comparison with DNS by Lee & Moser (2015), (*b*) $\langle \epsilon \rangle$-budget terms in comparison with R1000H.

wall-normal direction in the runs listed in table 1 is smaller than or similar to η, those in the wall-parallel directions are larger than η. Therefore, particular attention was paid to the influence of grid widths Δx and Δz.

Figure 2(*a*) shows a comparison of k-budget terms by R1000L and DNS by Lee & Moser (2015) at $Re_\tau = 1000$, here $k(= \langle u_\alpha u_\alpha \rangle /2)$ is the mean turbulent kinetic energy per unit mass. The grid widths $(\Delta x)^+ = 18.5$, $(\Delta z)^+ = 8.9$ in the former are larger than $(\Delta x)^+ = 10.9$, $(\Delta z)^+ = 4.6$ in the latter. Figure 2(*b*) shows a comparison of the mean energy dissipation rate ($\langle \epsilon \rangle$)-budget terms of R1000L and R1000H that is with finer resolution $(\Delta x)^+ = 7.8$, $(\Delta z)^+ = 4.2$. (The data of $\langle \epsilon \rangle$-budget terms for such a comparison are not available in Lee & Moser 2015.) The definition of the k- and $\langle \epsilon \rangle$-budget terms used in the figures is given in Appendix A (k is not wavenumber in this section nor in Appendix A).

In both figures 2(*a*) and 2(*b*), it is observed that the statistics of R1000L with lower resolution $(\Delta x)^+ = 18.5$, $(\Delta z)^+ = 8.9$ agree well with those of DNSs with higher resolution. The Kolmogorov length scale η is generally a function of Re_τ and y. At a given y, the scale η at higher Re_τ is similar to η at smaller Re_τ in the region including the inertial sublayer, as shown in Morishita, Ishihara & Kaneda (2019) and Lee & Moser (2019). This result and table 1 imply that the grid width in units of η of all the runs at $Re_\tau \geq 1000$ listed in table 1 is similar to that in R1000L. The agreement of the k- and $\langle \epsilon \rangle$-budget terms of

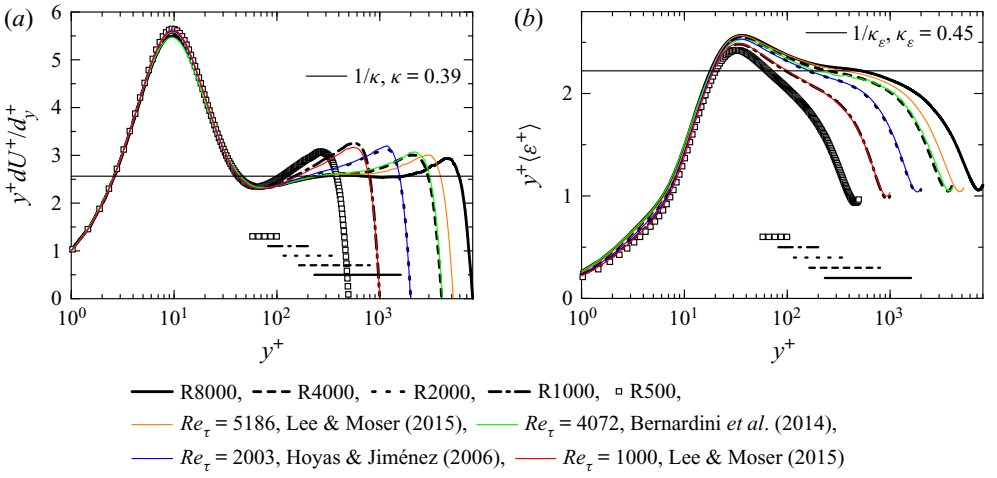

Figure 3. Normalised mean velocity gradient and energy dissipation rate, (*a*) $(\mathrm{d}U^+/\mathrm{d}y^+)y^+$ vs y^+. Thin solid straight lines represent $(\mathrm{d}U^+/\mathrm{d}y^+)y^+$ with $\kappa = 0.39$, (*b*) $\langle\epsilon\rangle^+ y^+$ vs y^+. Thin solid straight lines correspond to $\langle\epsilon\rangle^+ y^+ = 1/\kappa_\epsilon$ with $\kappa_\epsilon = 0.45$. Thick straight lines show the ranges $y^+ \in [2.6Re_\tau^{1/2}, 0.2Re_\tau]$.

R1000L with those of DNSs with higher resolution is encouraging for us to use the DNS data for the analysis of the second-order moments of the fluctuating velocity gradients.

3.2. *Mean flow, energy dissipation rate and ratio γ*

Figures 3(*a*) and 3(*b*) confirm (2.40) and (2.41), where data by DNSs with larger computational domains (Lee & Moser 2015; Hoyas & Jiménez 2006; Bernardini, Pirozzoli & Orlandi 2014) are also plotted as coloured lines (ϵ given by (2.33) was used in Bernardini *et al.* 2014). Figure 3(*a*) demonstrates that the mean flow profile $U(y)$ fits (2.40) well in a certain range of y^+, especially for R8000. Figure 3(*b*) shows that, although the approximation (2.41) for $\langle\epsilon\rangle$ is not as good as the approximation (2.40) for $U(y)$, the y-dependence of $\langle\epsilon\rangle\, y$ in the DNS is fairly weak in that range. In this sense, the results shown in figures 3(*a*) and 3(*b*) agree with the observations in Kaneda, Morishita & Ishihara (2013), Abe & Antonia (2016), Morishita *et al.* (2019) and Lee & Moser (2019) (Kaneda *et al.* (2013) and Morishita *et al.* (2019) used ϵ given by (2.33)).

Figures 3(*a*) and 3(*b*) show that the DNS profiles of $U(y)$ and $\langle\epsilon\rangle(y)$ depend on Re_τ and they approach those obtained from simple theories such as (2.40) and (2.41) with an increase in Re_τ. Readers may refer to Jiménez & Moser (2007) and Abe & Antonia (2016) for theories on the influence of finite Re_τ on $U(y)$ and $\langle\epsilon\rangle(y)$, respectively.

A least squares fit of (2.40) and (2.41) to the DNS data in the range $y^+ \in [2.6Re_\tau^{1/2}, 0.2Re_\tau]$ (Klewicki 2010; Chin *et al.* 2014) for the run at $Re_\tau \approx 8000$, for which $[2.6Re_\tau^{1/2}, 0.2Re_\tau] \approx [232, 1600]$, gives

$$\kappa = 0.39, \quad \kappa_\epsilon = 0.45, \quad K \equiv \frac{\kappa_\epsilon^{1/2}}{\kappa} = 1.72. \tag{3.1a–c}$$

Figure 4(*a*) plots γ as a function of y^+ and confirms that, in each run, there is a range of y where γ is small. The existence of such a range is a prerequisite for the theory proposed in § 2. In figure 4(*b*), γ in each run is seen to scale well with $(y^+)^{-1/2}$ in an appropriate range, in accordance with (2.42).

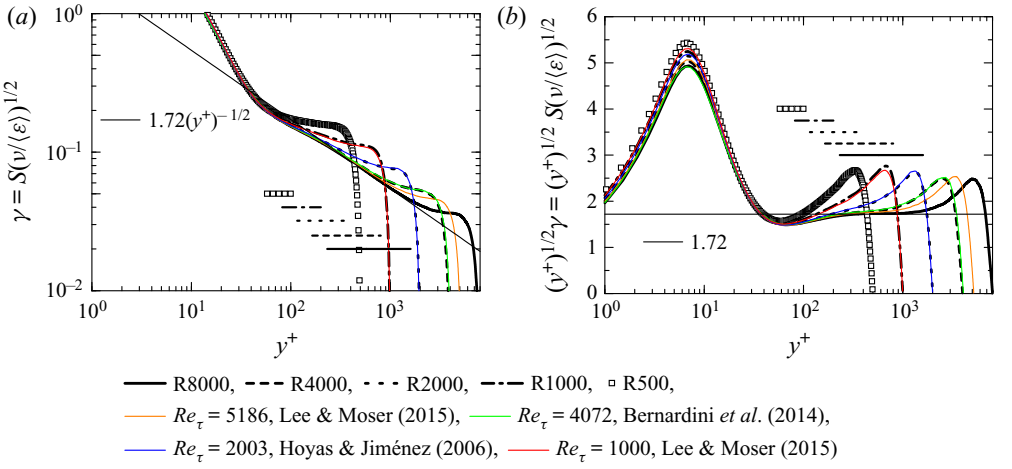

Figure 4. (*a*) Ratio γ vs y^+, (*b*) $y^{+1/2}\gamma$ vs y^+. Thin solid straight lines show $\gamma = K(y^+)^{-1/2}$ with $K = 1.72$. The meaning of thick straight lines is the same as in figure 3.

3.3. *Second-order moments of g_{ij}*

Figures 5(*a*,*c*,*e*) and 5(*b*,*d*,*f*) show the moments $(\nu/\langle\epsilon\rangle)\langle g_{ii}^2\rangle$ and the anisotropy correction $|(\nu/\langle\epsilon\rangle)\langle g_{ii}^2\rangle - 1/15|$ for $i, j = 1, 2$ and 3, as functions of y^+, respectively. Figure 5(*a*,*c*,*e*) displays that, with an increase in y^+, i.e. a decrease of γ, the moments approach the constant $1/15$ in an appropriate range of y^+. This is in accordance with (2.44). The slope of anisotropy correction for $i = 1$ in figure 5(*b*,*d*,*f*) is approximately $-1/2$, in accordance with (2.44). The slope $-1/2$ for $i = 1$ agrees with the value by Lee & Moser (2019), who computed $(1 - 15\nu\langle g_{11}^2\rangle/\langle\epsilon\rangle)$ and noted that it varies in a manner similar to $(y^+)^{-1/2}$. This slope $-1/2$ for $i = 1$ agrees with the value by Lee & Moser (2019), who computed $(1 - 15\nu\langle g_{11}^2\rangle/\langle\epsilon\rangle)$ and noted that it varies in a manner similar to $(y^+)^{-1/2}$.

Figure 5(*b*,*d*,*f*) shows that the moments $(\nu/\langle\epsilon\rangle)\langle g_{ii}^2\rangle$ for $i = 2$ and 3 approach the isotropy value of $1/15$ with an increase in y^+, and the approaches are considerably faster than that of $(\nu/\langle\epsilon\rangle)\langle g_{11}^2\rangle$. Correspondingly to this difference, the anisotropy corrections $|(\nu/\langle\epsilon\rangle)\langle g_{ii}^2\rangle - 1/15|$ for $i = 2, 3$ seen in figure 5(*b*,*d*,*f*) are considerably smaller than the correction for $i = 1$. This suggests that the anisotropy correction coefficients $C_{1,iiii}$ for $i = 2, 3$ are considerably smaller than $C_{1,1111}$.

One might think that the agreement of (2.44) with the DNS is poor. However, it is to be recalled that terms of $O(\gamma^1)$ are discarded in (2.35) and (2.44). The discarded terms may not be negligible compared with the $C_{1,iiii}$-term for $i = 2, 3$. If this is the case, then the departure of the DNS curves from the $(y^+)^{-1/2}$ scaling would be not surprising.

Figure 6 displays the moments $(\nu/\langle\epsilon\rangle)\langle(g_{ij})^2\rangle$ for $i, j = 1, 2$ and 3 with $i \neq j$ and figure 7 shows the same but for the anisotropy corrections $|(\nu/\langle\epsilon\rangle)\langle(g_{ij})^2\rangle - 2/15|$. In accordance with (2.45), all moments in figure 6 approach the isotropy value $2/15$ and the slopes of the moments in figure 6 are approximately $-1/2$ except for $(i, j) = (2, 3)$. The smallness of the anisotropy correction value for $(i, j) = (2, 3)$ compared with those for the other set of (i, j) observed in figure 7 suggests that the difference of the slopes for $(i, j) = (2, 3)$ by DNS and the theory in (2.45) is due to the smallness of the anisotropy correction coefficient $C_{1,ijij}$.

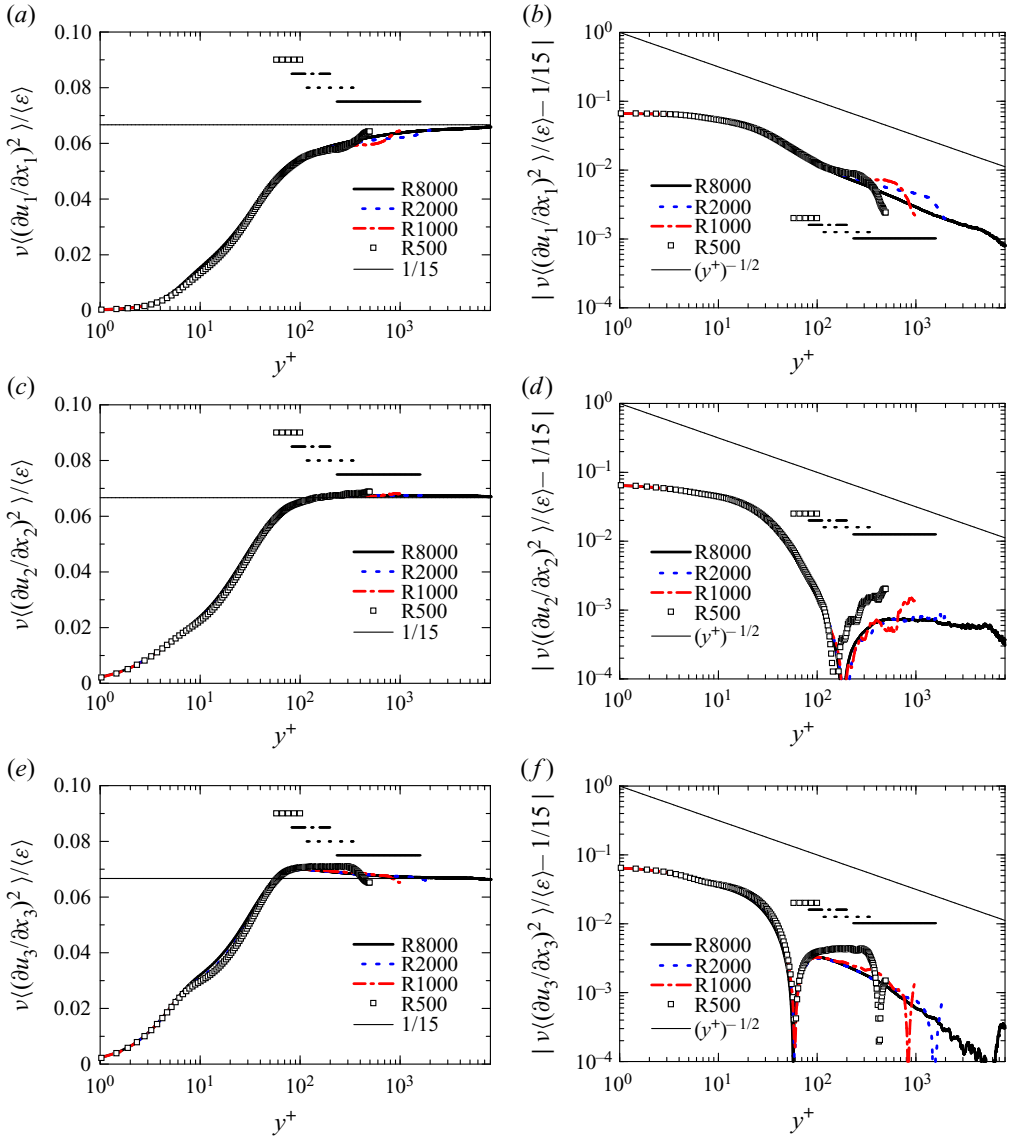

Figure 5. (*a*,*c*,*e*) Value of $\nu\langle(g_{ii})^2\rangle/\langle\epsilon\rangle$ vs y^+ for $i = 1, 2$ and 3. (*b*,*d*,*f*) The same as (*a*,*c*,*e*) but for $|\nu\langle(g_{ii})^2\rangle/\langle\epsilon\rangle - 1/15|$. Thin solid straight lines in (*a*,*c*,*e*) and (*b*,*d*,*f*), respectively, show $\nu\langle(g_{ii})^2\rangle/\langle\epsilon\rangle = 1/15$ and the slope $-1/2$. The meaning of thick straight lines is the same as in figure 3.

Let λ_{ijk} be the length scale (Taylor microlength scale) defined by

$$\frac{1}{(\lambda_{ijk})^2}\langle u_i(\boldsymbol{x})u_j(\boldsymbol{x})\rangle = -\frac{\partial^2}{\partial r_k^2}\langle u_i(\boldsymbol{x})u_j(\boldsymbol{x}+\boldsymbol{r})\rangle\bigg|_{\boldsymbol{r}=0}. \tag{3.2}$$

These length scales are a generalisation of those studied by Vreman & Kuerten (2014) who computed $\lambda_i \equiv \lambda_{iii}$ in DNS with Re_τ up to 590. In TCF, in which the statistics of the

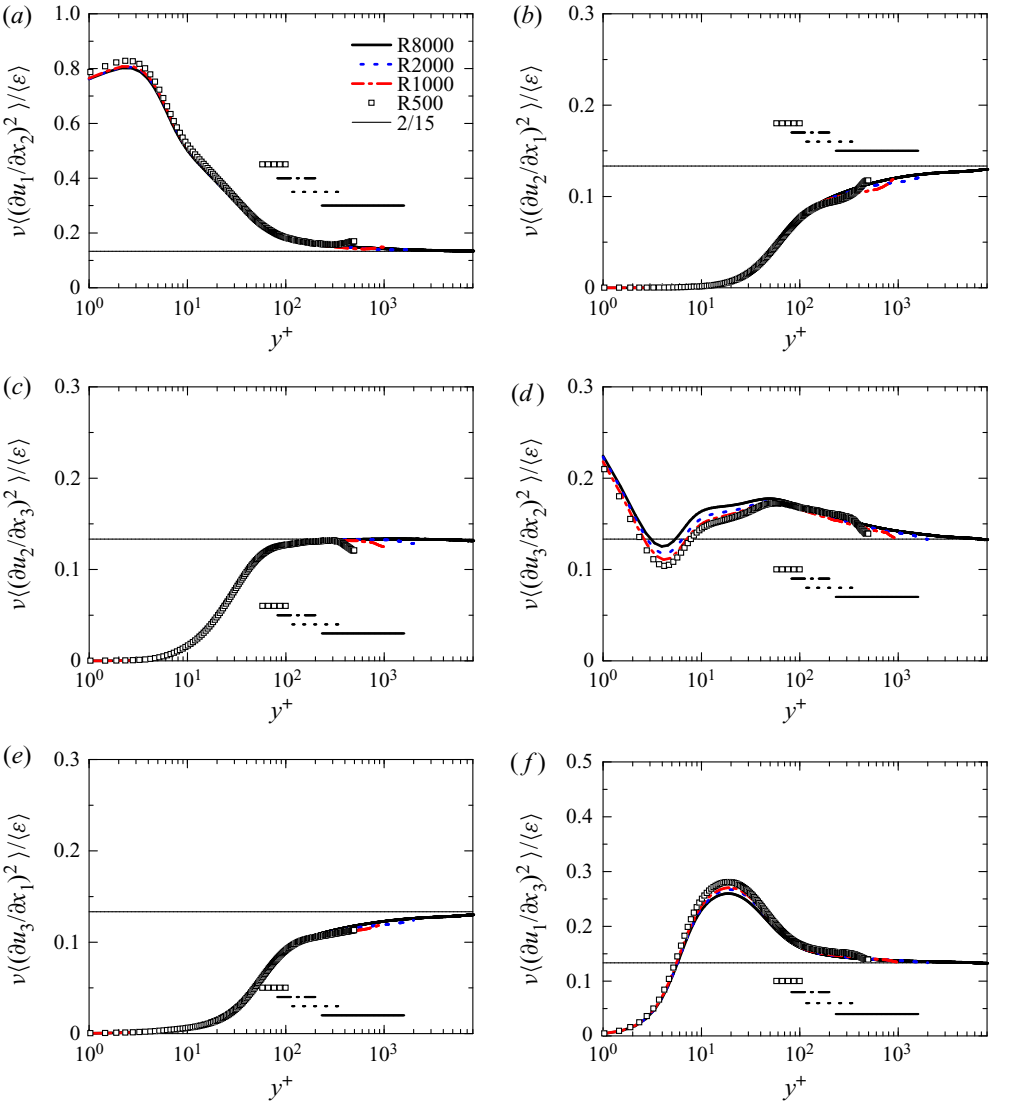

Figure 6. Value of $\nu\left\langle(g_{ij})^2\right\rangle/\langle\epsilon\rangle$ vs y^+ for (*a*) $(i,j)=(1,2)$, (*b*) $(i,j)=(2,1)$, (*c*) $(i,j)=(2,3)$, (*d*) $(i,j)=(3,2)$, (*e*) $(i,j)=(3,1)$, (*f*) $(i,j)=(1,3)$. Thin solid straight lines show $\nu\left\langle(g_{ij})^2\right\rangle/\langle\epsilon\rangle=2/15$. The meaning of thick lines is the same as in figure 3.

fluctuating field $\boldsymbol{u}$ are homogeneous in the x_1 and x_3 directions, we have

$$-\frac{\partial^2}{\partial r_k^2}\left\langle u_i(\boldsymbol{x})u_j(\boldsymbol{x}+\boldsymbol{r})\right\rangle\Big|_{\boldsymbol{r}=0}=-\delta_{k2}\frac{\partial}{\partial x_2}\left\langle u_i(\boldsymbol{x})\frac{\partial}{\partial x_2}u_j(\boldsymbol{x})\right\rangle+C_{ikjk}(\boldsymbol{x}). \tag{3.3}$$

If the inhomogeneity in the x_2 direction is weak so that the first term on the right-hand side of (3.3) and the x_2-dependence of $\left\langle u_i(\boldsymbol{x})u_j(\boldsymbol{x})\right\rangle$ are negligible, then (3.2) and (3.3) with (2.41) and (2.44), (2.45) yield $\lambda_{iik}\propto(y^+)^{1/2}$. This is consistent with the results by Morishita *et al.* (2019), who computed λ_{iik} (in the present notation) in DNSs of TCF with Re_τ up to ≈ 5200.

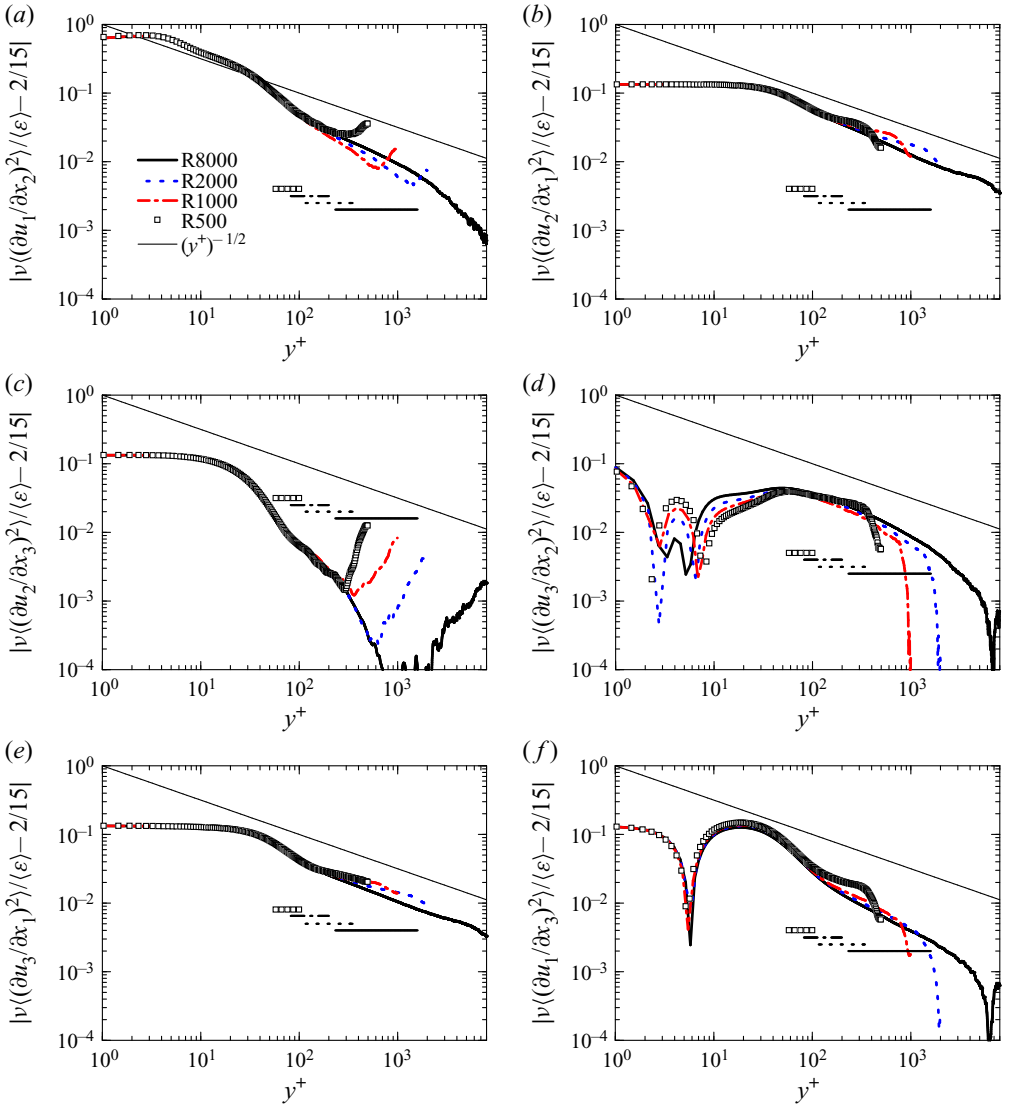

Figure 7. Same as in figure 6, but for $|\nu\langle(g_{ij})^2\rangle/\langle\epsilon\rangle - 2/15|$. Thin solid straight lines show the slope $-1/2$. The meaning of thick lines is the same as in figure 3; (*a*) $(i,j) = (1,2)$, (*b*) $(i,j) = (2,1)$, (*c*) $(i,j) = (2,3)$, (*d*) $(i,j) = (3,2)$, (*e*) $(i,j) = (3,1)$, (*f*) $(i,j) = (1,3)$.

Figure 8 displays the moments $(\langle\epsilon\rangle/\nu)\langle g_{1j}g_{2j}\rangle = (\langle\epsilon\rangle/\nu)\langle g_{2j}g_{1j}\rangle$. In view of the geometrical symmetry of TCF, it is natural to assume that $\langle u_3(x,y,z))u_k(x+x',y+y',z)\rangle = 0$ and $\langle u_3(x,y,z))u_k(x,y,z+z')\rangle = 0$ is odd in z' for any x, y, z and (x', y') if $k = 1$ or 2, so that $\langle g_{ij}g_{kj}\rangle = 0$ unless $(i,k) = (1,2)$ or $(2,1)$. Therefore, these moments are not shown here unless $(i,k) = (1,2)$ or $(2,1)$. It is observed that the slope of $(\langle\epsilon\rangle/\nu)\langle g_{13}g_{23}\rangle$ is approximately $-1/2$ in an appropriate range of y^+ (e.g. $y^+ \sim 10^3$) in the run with $Re_\tau \approx 8000$, in accordance with (2.46). The difference of the slopes from (2.46) for $j = 1$ and 2 is presumably due to the smallness of the anisotropy correction coefficient $C_{1,1j2j}$ for $j = 1$ and 2.

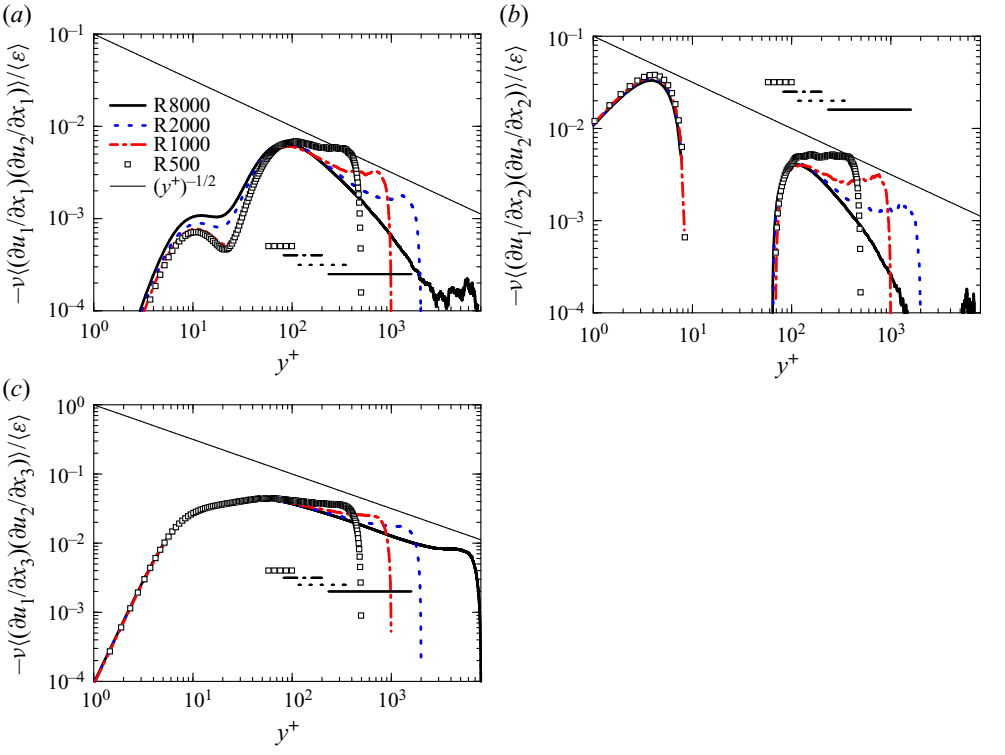

Figure 8. Value of $\nu\left\langle(g_{ij}g_{kj})\right\rangle/\langle\epsilon\rangle$ vs y^+ for $(i,k)=(1,2)$ and $j=1,2,3$; (a) $j=1$, (b) $j=2$ and (c) $j=3$. Thin solid straight lines show the slope $-1/2$. The meaning of thick lines is the same as in figure 3.

Figure 9 presents the ratios $\left\langle(g_{ij})^2\right\rangle/\left\langle(g_{ii})^2\right\rangle$ for $i,j=1,2$, and 3 with $i\neq j$. It is observed that, with an increase in y^+ i.e. with a decrease in γ, they approach the isotropy value of two, in accordance with the theoretical conjecture (2.47). The results in figure 9 are consistent with those in Pumir *et al.* (2016) who computed the ratios $\xi_i\equiv\left\langle(\partial u_1/\partial x_i)^2\right\rangle/\left\langle(\partial u_1/\partial x_1)^2\right\rangle$ in the DNS of TCF at $Re_\tau\approx 1000$ and showed that the ratios ξ_2 and ξ_3 decrease towards two near the centre of the channel in the DNS.

Figure 10 displays the anisotropy corrections $|\left\langle(g_{ij})^2\right\rangle/\left\langle(g_{ii})^2\right\rangle-2|$ for $i,j=1,2$ and 3 with $i\neq j$. The slopes at large y^+ are close to $-1/2$ in accordance with (2.47), except for $(i,j)=(2,3)$. The difference in the slope from (2.47) for $(i,j)=(2,3)$ is presumably due to the smallness of the anisotropy correction coefficient $C_{1,12323}$, as suggested by the curve for $(i,j)=(2,3)$ in figure 7(*c*) and the fast approach to 2 in the curve for $(i,j)=(2,3)$ in figure 9(*d*).

3.4. *Energy dissipation rate tensor*

Figure 11(*a*,*b*,*c*) presents $\epsilon_{ii}/(2\langle\epsilon\rangle)$ for $i=1,2$ and 3. Additionally, figure 12 shows the magnitude of the deviatoric parts d_{ij} of $\epsilon_{ij}/(2\langle\epsilon\rangle)$ for $\{i,j\}=\{1,2,3\}$, where

$$d_{ij}\equiv\frac{\epsilon_{ij}}{2\langle\epsilon\rangle}-\frac{1}{3}\delta_{ij}. \tag{3.4}$$

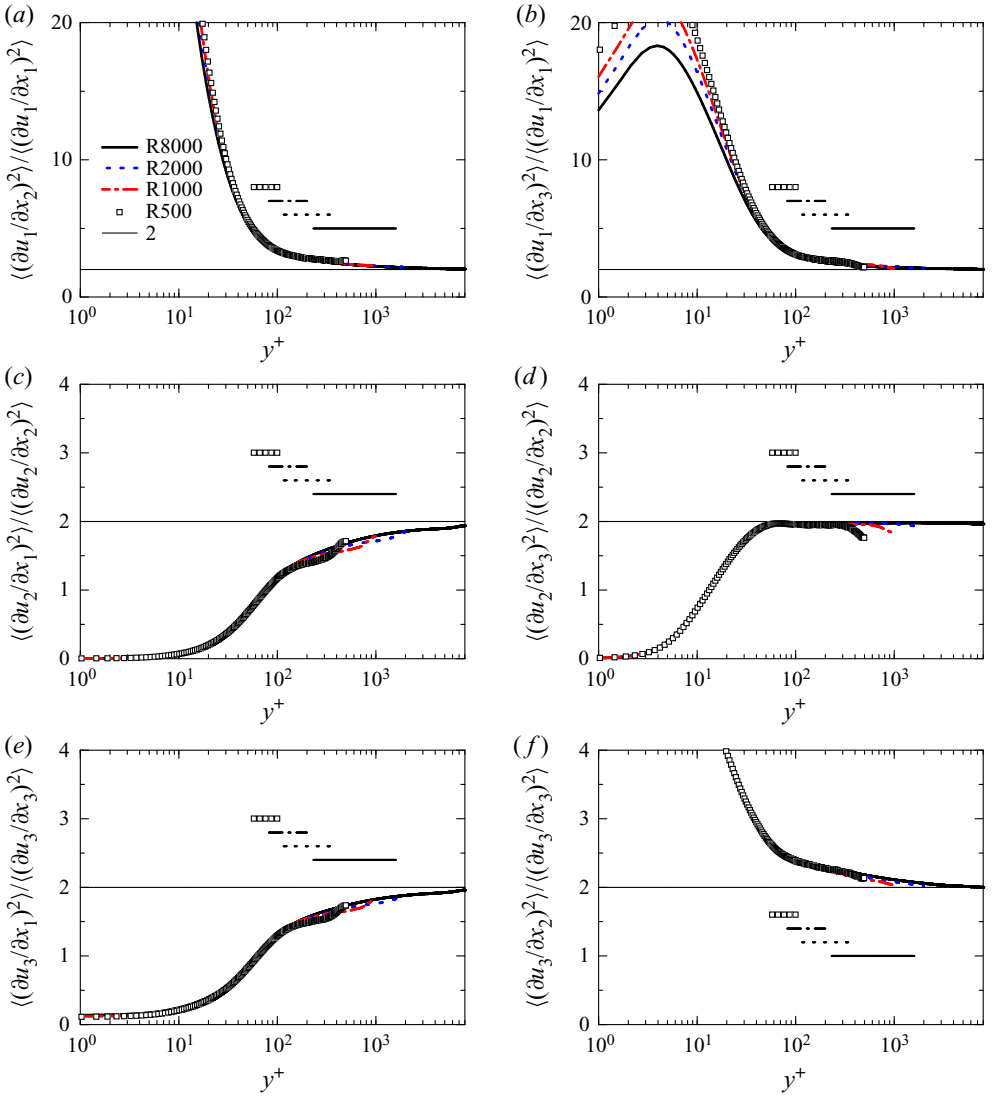

Figure 9. Ratios $\langle(g_{ij})^2\rangle/\langle(g_{ii})^2\rangle$ vs y^+ for $i,j = 1, 2$ and 3 with $i \neq j$; (*a*) $(i,j) = (1,2)$, (*b*) $(i,j) = (1,3)$, (*c*) $(i,j) = (2,1)$, (*d*) $(i,j) = (2,3)$, (*e*) $(i,j) = (3,1)$, (*f*) $(i,j) = (3,2)$. Thin solid straight lines show $\langle(g_{ij})^2\rangle/\langle(g_{ii})^2\rangle = 2$. The meaning of thick lines is the same as in figure 3.

As noted above, a consideration of the geometrical symmetry of TCF gives $\langle g_{ik}g_{ik}\rangle = 0$, so that $d_{ij} = 0$ if $(i,j) = (2,3)$, $(3,2)$, $(3,1)$ or $(1,3)$. Therefore, d_{23}, d_{32}, d_{13} and d_{31} are not plotted in figure 12.

Figure 11(*a*,*b*,*c*) demonstrates that $\epsilon_{ii}/(2\langle\epsilon\rangle)$ for $i = 1, 2$ and 3 approach the isotropy value of $1/3$ with an increase in y^+ in accordance with (2.48). The slopes of d_{11} and d_{22} from the DNS at $y^+ \sim 10^3$ are approximately $-1/2$ in accordance with (2.48). Regarding d_{33} in figure 12(*c*), the departure of the slope from $-1/2$ is presumably due to the smallness of $C_{1,3\alpha3\alpha}$.

Using the data of a series of DNSs of TCF with Re_τ up to 5200, Lee & Moser (2019) computed the second invariant II_ϵ of d_{ij} as suggested by Antonia *et al.* (1991) and Antonia,

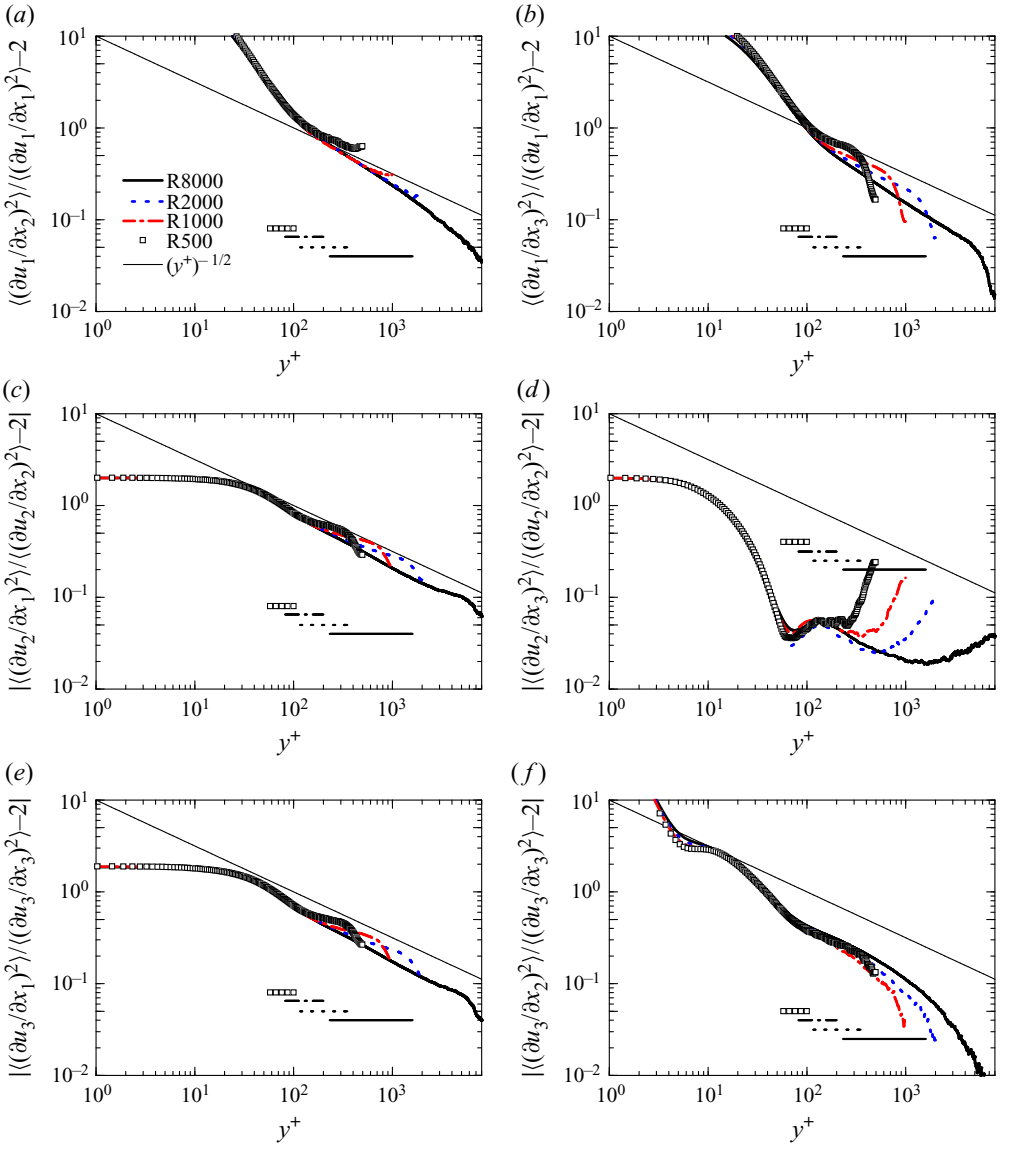

Figure 10. Same as figure 9, but for $|\langle(g_{ij})^2\rangle / \langle g_{ii})^2\rangle - 2|$. Thin solid straight lines show the slope $-1/2$. The meaning of thick lines is the same as in figure 3; (*a*) $(i, j) = (1, 2)$, (*b*) $(i, j) = (1, 3)$, (*c*) $(i, j) = (2, 1)$, (*d*) $(i, j) = (2, 3)$, (*e*) $(i, j) = (3, 1)$, (*f*) $(i, j) = (3, 2)$.

Djenidi & Spalart (1994), which is given in the present notation as

$$II_\epsilon \equiv \tfrac{1}{2} d_{\alpha\beta} d_{\beta\alpha} = \tfrac{1}{2}\left[(d_{11})^2 + (d_{22})^2 + (d_{33})^2 + 2(d_{12})^2\right]. \tag{3.5}$$

They noted that, in the overlap region ($y^+ \approx 100$ to $y/\delta \approx 0.2$), II_ϵ varies as $(y^+)^{-5/4}$, where 2δ is the channel width. This exponent $-5/4$ appears to be consistent with figure 13(*a*).

In contrast, (2.39), (2.48), (3.4) and (3.5) give

$$II_\epsilon \approx C_{II}\gamma^2, \tag{3.6}$$

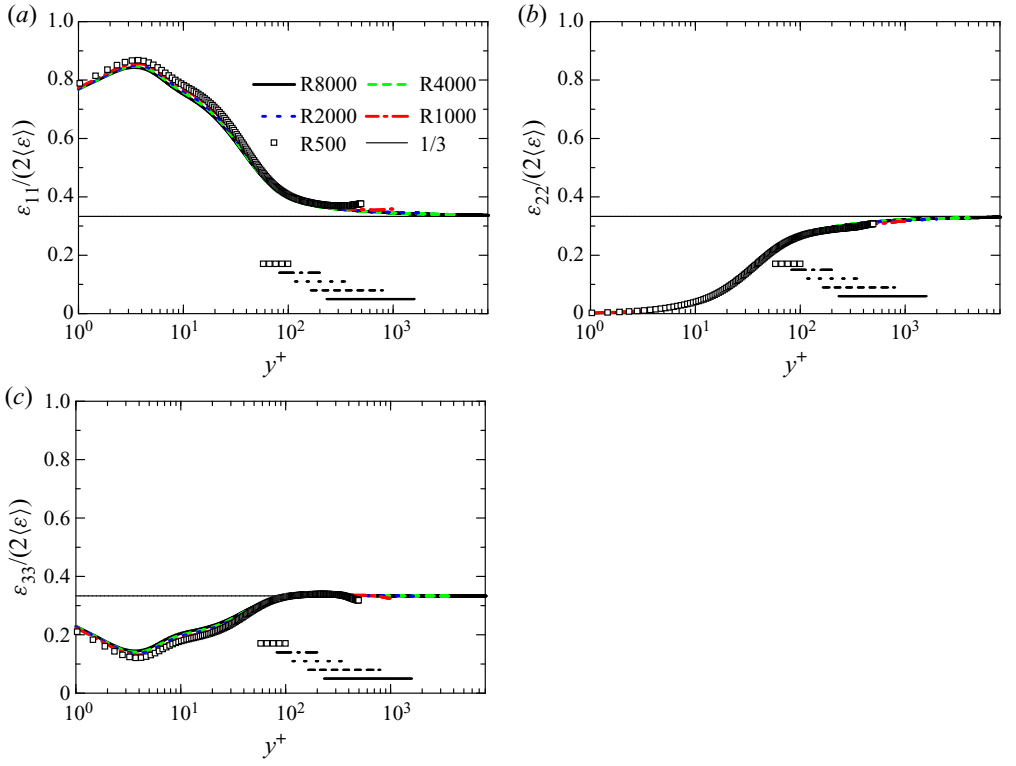

Figure 11. Values of $\epsilon_{ii}/(2\langle\epsilon\rangle)$ for $i = 1, 2$ and 3 vs y^+. Thin solid straight lines show $\epsilon_{ii}/(2\langle\epsilon\rangle) = 1/3$. The meaning of thick lines is the same as in figure 3.

and $II_\epsilon \propto (y^+)^{-1}$ for large y^+, where C_{II} is a dimensionless constant determined using the constants $C_{1,ijkj}$. Thus, the slope obtained by (2.48) appears to be in conflict with that obtained by DNS. However, it is to be recalled that (2.39) is based on (2.27), which discards possible corrections of the $O(\gamma)$ terms for small γ to $\Delta\langle g_{ij}g_{mn}\cdots\rangle$, as well as corrections due to effects other than the mean shear, which are not taken into account by the parameter γ.

As regards the correction, say $\Delta_{2\gamma}$, to $\Delta\langle g_{ij}g_{mn}\rangle$ by terms of $O(\gamma)$, a naive idea suggests that one may approximate it by a term such as $c_2\gamma^\alpha$, where c_2 and $\alpha(>1)$ are constants. If one simply puts $\alpha = 2$, then the addition of the correction term $c_2\gamma^2$ to (2.27) gives

$$II_\epsilon \approx C_{II}\gamma^2 + D_{II}\gamma^3. \tag{3.7}$$

Substitution of (2.42) into (3.7) gives

$$II_\epsilon \approx C_{II}(y^+)^{-1} + D'_{II}(y^+)^{-\beta}, \quad (\beta = 3/2), \tag{3.8}$$

where C_{II}, D_{II} and D'_{II} are dimensionless constants, and $D'_{II} = CD_{II}$. Here, terms of $O(\gamma^3)$ in (3.7) and $O((y^+)^{-\beta})$ in (3.8) are ignored.

Regarding possible corrections by effects other than the mean shear, one can consider those related to the finiteness of the distance, say y, from the wall. In this respect, it is of interest to note that (2.43) gives $\eta/y \propto (y^+)^{-3/4}$ in the inertial sublayer. If one assumes (i) that such a correction, say Δ_w, due to the finiteness of $1/y$ is linear in $1/y$, so that it is given by the form $\Delta_w \approx c'_w/y$ as a first approximation, and (ii) that the coefficient c'_w

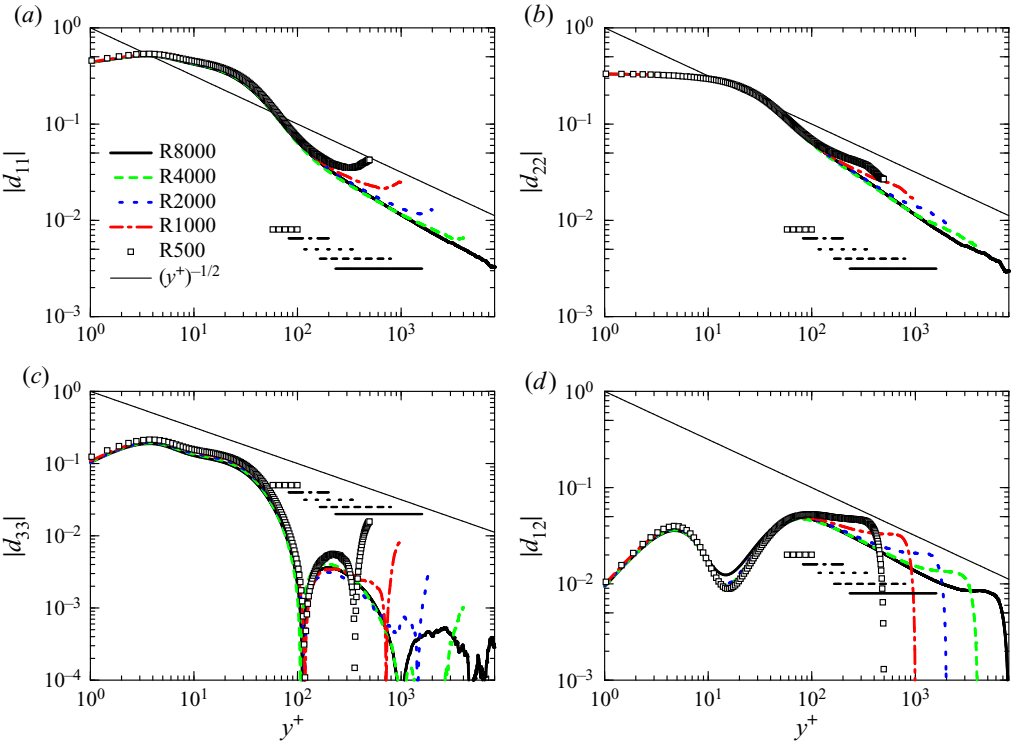

Figure 12. Values of $|d_{11}|$, $|d_{22}|$, $|d_{33}|$ and $|d_{12}| = |d_{21}|$. Thin solid straight lines show the slope $-1/2$. The meaning of thick lines is the same as in figure 3.

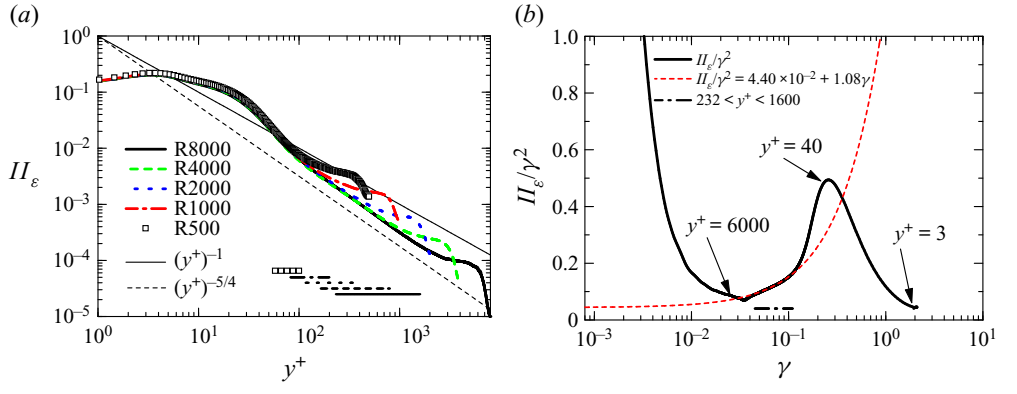

Figure 13. (*a*) Second invariant II_ϵ of tensor (d_{ij}). Thin solid straight and dotted straight lines denote the slopes -1 and $-5/4$, respectively. (*b*) Value of II_ϵ/γ^2 vs γ; broken lines represent the fit (3.7) with $C_{II} = 4.40 \times 10^{-2}$ and $D_{II} = 1.08$. The meaning of thick lines is the same as in figure 3.

depends only on ν and $\langle\epsilon\rangle$, then one has $c'_w \propto \eta$, so that $\Delta_w \approx c_w(y^+)^{-3/4}$, where c_w is a dimensionless constant. The addition of such correction term to (2.27) gives II_ϵ but with $\beta = 5/4$.

It is of interest to ask how much the difference between the theory and DNS is attributable to these corrections. Figures 13 and 14 may give an idea on this question. Figure 13(*b*) shows II_ϵ/γ^2 vs γ. A least squares fit of II_ϵ/γ^2 given by (3.7) with $\beta = 3/2$

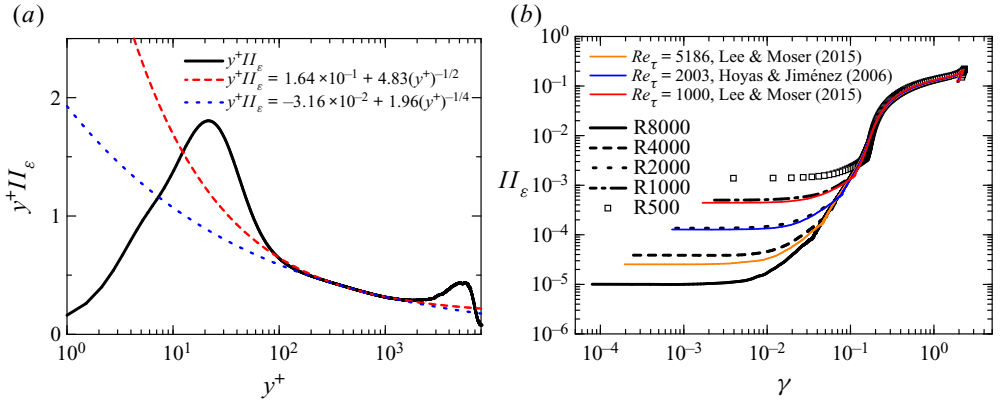

Figure 14. (*a*) Value of $II_\epsilon y^+$ vs y^+. Broken line shows the fit (3.8) with $\beta = 3/2$, $C_{II} = 1.64 \times 10^{-1}$ and $D'_{II} = 4.83$, and the dotted line displays the fit (3.8) with $\beta = 5/4$, $C_{II} = -3.16 \times 10^{-2}$ and $D'_{II} = 1, 96$, and (*b*) II_ϵ vs γ.

to the DNS data in the range of γ that corresponds to the range $y^+ \in [232, 1600]$ provides

$$C_{II} = 4.40 \times 10^{-2}, \quad D_{II} = 1.08. \tag{3.9a,b}$$

The value given by (3.7) with (3.9*a*,*b*) is plotted together with the DNS data. It is observed that II_ϵ is well approximated by (3.7) in a certain range of γ.

Figure 14(*a*) shows $II_\epsilon y^+$ vs y^+. A least squares fit of $II_\epsilon y^+$ given by (3.8) with $\beta = 3/2$ and 5/4 to the DNS data in the range of $y^+ \in [2.6Re_\tau^{1/2}, 0.2Re_\tau] \approx [232, 1600]$ gives

$$\beta = 3/2;\ C_{II} = 1.64 \times 10^{-1}, \quad D'_{II} = 4.83, \tag{3.10a,b}$$

$$\beta = 5/4;\ C_{II} = -3.16 \times 10^{-2}, \quad D'_{II} = 1.96. \tag{3.11a,b}$$

The values given by (3.8) with (3.10*a*,*b*) and (3.11*a*,*b*) are plotted in figure 14(*a*) together with the DNS data. It is observed that $II_\epsilon y^+$ is well approximated by (3.8) in the range of $y^+ \in [232, 1600]$. This result suggests that the difference between the slope $-5/4$ observed in DNS data and -1 by the theory is attributable at least partly to the finiteness of γ. However, the possibility that the slope $-5/4$ is an intrinsic feature and remains constant $-5/4$ in an appropriate range of y^+ at $Re_\tau \to \infty$ is not excluded, and the question of how to fix the best value of the exponent β in (3.8) is not yet settled.

Figure 13(*a*) shows that, at small γ, (e.g. $\gamma < 0.03$), DNS data for II_ϵ/γ^2 do not fit well to (3.6), but blow up like $\propto \gamma^m$ with $m \approx -2$. This result implies that $II_\epsilon \approx$ constant, in the small$-\gamma$ range, as confirmed by figure 14(*b*), which shows II_ϵ vs γ. This disagreement of DNS data with (3.6) is not surprising because the anisotropy in ϵ_{ij} can in general be induced not only by the mean shear, but also by other factors, in particular the anisotropy of energy-containing eddies, while the effect of the latter is assumed to be negligible compared with those of the former in the derivation of (3.6). In the central region of the channel, the statistics of the large-scale eddies are anisotropic, and their influence on small-scale statistics can remain finite, even if γ is very small. This implies that, in this region, the anisotropy measure II_ϵ can remain finite, independently of the smallness of γ. This picture is consistent with figure 14(*b*), which shows that II_ϵ is small but finite at $\gamma \ll 1$.

4. Discussion and conclusions

4.1. *Influence of large-scale eddies*

As noted in the last paragraph of § 2.1, we assumed in this study that the influence of the anisotropy in energy-containing eddies on the statistics at scales $\sim \eta$ is not significant, or at most of similar order compared with the effect of the mean shear. In this subsection, we consider in some details about the possible influence of the anisotropy in energy containing eddies.

In order to get some idea on the influence, it is instructive to decompose the fluctuating field $\boldsymbol{u}$ as

$$\boldsymbol{u} = \boldsymbol{u}^L + \boldsymbol{u}^S, \tag{4.1}$$

where $\boldsymbol{u}^L$ and $\boldsymbol{u}^S$, respectively, represent the fluctuating velocity components by large-scale eddies of the energy-containing range and by the other smaller eddies. Correspondingly to this decomposition, $\boldsymbol{v}$ can be decomposed as

$$\boldsymbol{v} = \boldsymbol{v}^L + \boldsymbol{v}^S, \tag{4.2}$$

so that the first three terms on the right-hand side of (2.7) can be written as

$$(\boldsymbol{V}\cdot\boldsymbol{\nabla})\boldsymbol{v} = (\boldsymbol{V}\cdot\boldsymbol{\nabla})\boldsymbol{v}^L + (\boldsymbol{V}\cdot\boldsymbol{\nabla})\boldsymbol{v}^S, \tag{4.3}$$

$$(\boldsymbol{v}\cdot\boldsymbol{\nabla})\boldsymbol{V} = (\boldsymbol{v}^L\cdot\boldsymbol{\nabla})\boldsymbol{V} + (\boldsymbol{v}^S\cdot\boldsymbol{\nabla})\boldsymbol{V}, \tag{4.4}$$

$$(\boldsymbol{v}\cdot\boldsymbol{\nabla})\boldsymbol{v} = (\boldsymbol{v}^L\cdot\boldsymbol{\nabla})\boldsymbol{v}^L + (\boldsymbol{v}^L\cdot\boldsymbol{\nabla})\boldsymbol{v}^S + (\boldsymbol{v}^S\cdot\boldsymbol{\nabla})\boldsymbol{v}^L + (\boldsymbol{v}^S\cdot\boldsymbol{\nabla})\boldsymbol{v}^S, \tag{4.5}$$

where $\boldsymbol{v}^L(\boldsymbol{r}, s) \equiv \boldsymbol{u}^L(\boldsymbol{r}+\boldsymbol{r}_0, s+t_0) - \boldsymbol{u}^L(\boldsymbol{x}_0, t_0)$ and $\boldsymbol{v}^S(\boldsymbol{r}, s) \equiv \boldsymbol{u}^S(\boldsymbol{r}+\boldsymbol{r}_0, s+t_0) - \boldsymbol{u}^S(\boldsymbol{x}_0, t_0)$. Simple order estimates (see Appendix B) of the terms on the right-hand sides of (4.3)–(4.5) show that

$$(\boldsymbol{v}^L\cdot\boldsymbol{\nabla})\boldsymbol{v}^S \sim (\boldsymbol{v}^S\cdot\boldsymbol{\nabla})\boldsymbol{v}^L \sim \gamma_e(\boldsymbol{v}^S\cdot\boldsymbol{\nabla})\boldsymbol{v}^S, \tag{4.6}$$

and that the order of the magnitude of each of the other terms including $\boldsymbol{v}^L$ is smaller than that of $(\boldsymbol{v}^L\cdot\boldsymbol{\nabla})\boldsymbol{v}^S \sim (\boldsymbol{v}^S\cdot\boldsymbol{\nabla})\boldsymbol{v}^L$ provided that $\gamma_e \ll 1$ and $\gamma \ll 1$, where γ_e is the ratio of the time scale $\tau_\eta \equiv \eta/v_\eta$ of small eddies of size $\sim \eta$ to the time scale $\tau_E \equiv \ell/u'$ of energy-containing eddies, i.e.

$$\gamma_e \equiv \frac{\eta/v_\eta}{\ell/u'} = \frac{u'}{\ell}\frac{\eta}{v_\eta}, \tag{4.7}$$

in which $3(u')^2 = \langle \boldsymbol{u}\cdot\boldsymbol{u}\rangle$, and ℓ is the characteristic length scale of the energy-containing eddies. This implies that, if $\gamma_e \ll 1$ and $\gamma \ll 1$, then the magnitude of the terms representing the influence of the large-scale fluctuating velocity field $\boldsymbol{v}^L$ in (2.7) is negligibly small compared with that of the nonlinear coupling term $(\boldsymbol{v}^S\cdot\boldsymbol{\nabla})\boldsymbol{v}^S \sim (\boldsymbol{v}\cdot\boldsymbol{\nabla})\boldsymbol{v}$ and the viscous term $\nu\nabla^2\boldsymbol{v}^S \sim \nu\nabla^2\boldsymbol{v}$.

The substitution of $\eta/v_\eta = (\nu/\langle\epsilon\rangle)^{1/2}$ into (4.7) gives

$$\gamma_e = \frac{u'}{\ell}\left(\frac{\nu}{\langle\epsilon\rangle}\right)^{1/2}. \tag{4.8}$$

Hence, if $\langle\epsilon\rangle \sim u'^3/\ell$, then we have $\gamma_e \sim Re_u^{-1/2}$, where $Re_u \equiv u'\ell/\nu$. This means that γ_e is small for large Re_u. Thus, the assumption of the smallness of the influence of the anisotropy of large-scale fluctuating eddies is acceptable, if Re_u is so large that γ_e given by (4.8) is sufficiently small.

If one may assume that in the inertial sublayer $u' \sim u_\tau$ and $\ell \sim y$, then (4.8) and (2.41) give $\gamma_e \sim (y^+)^{-1/2}$. This and (2.42) imply $\gamma_e \sim \gamma$ in the inertial sublayer. One might therefore think it questionable that the influence of $\boldsymbol{v}^L$, i.e. the influence of anisotropy of large-scale fluctuating eddies (LS-anisotropy) is negligible compared with that of mean shear (MS-anisotropy), in the inertial sublayer.

However, it is to be recalled that γ and γ_e are, respectively, proportional to the norm S of the tensor $(\partial U_i/\partial x_j)$ and approximately proportional to the magnitude of the large-sale fluctuating velocity $\boldsymbol{v}^L$, and that the average of $\boldsymbol{v}^L$, in contrast to those of $\partial U_i/\partial x_j$ and $\boldsymbol{V}$, is zero. This and the estimate (4.6) yield the conjecture that the influence on the small-scale statistics by LS-anisotropy is not as strong as that by MS-anisotropy, even if $\gamma \sim \gamma_e$.

4.2. *Assumption of linearity of* $\Delta_1 \langle B\rangle$ *in the tensor* $(\partial U_i/\partial x_j)$

In the second hypothesis of similarity for TSF proposed in § 2.1, we assumed that the change $\Delta\langle B\rangle$ of $\langle B\rangle$ owing to the mean shear can be approximated to be linear in the scalar γ, not in the tensor $(\partial U_i/\partial x_j)$, i.e. not in the tensor (γ_{ij}), for sufficiently small but finite γ, where

$$(\gamma_{ij}) \equiv \left(\frac{\nu}{\langle\epsilon\rangle}\right)^{1/2}\left(\frac{\partial U_i}{\partial x_j}\right). \tag{4.9}$$

Here, the tensor whose elements are given by $a_{ij\ldots}$ is denoted as $(a_{ij\ldots})$. In this subsection we consider the assumption of the linearity of $\Delta_1\langle B\rangle$ in $(\partial U_i/\partial x_j)$, i.e. in (γ_{ij}), instead of γ, where $\Delta_1\langle B\rangle$ is the leading order term(s) of $\Delta\langle B\rangle$ for small γ.

In a study of the response of the second-order velocity correlation spectra, say $\Delta Q_{ij}(\boldsymbol{k})$, in the ISR to small but finite mean shear, Ishihara *et al.* (2002) assumed the response to be approximately linear in the tensor $(\partial U_i/\partial x_j)$ (not the scalar S) under an appropriate normalization, where $\boldsymbol{k}$ is the wave vector. This gives $\Delta Q_{ij}(\boldsymbol{k}) \approx T_{ij\alpha\beta}(\boldsymbol{k})\partial U_\alpha/\partial x_\beta$ under certain assumptions, where $(T_{ij\alpha\beta})$ is an isotropic fourth-order tensor independent of $(\partial U_i/\partial x_j)$. They showed that it is in reasonable agreement with DNS of homogeneous TSF under simple mean shear.

From this, one might think that one may assume, instead of the second hypothesis (ii) proposed in § 2.1, the following modified hypothesis.

(m-ii) Modified second hypothesis of similarity for TSF.
For sufficiently small but finite γ, $\Delta\langle B\rangle$ can be approximated to be linear in the tensor (γ_{ij}), i.e. $\Delta\langle B\rangle \approx \Delta_1\langle B\rangle$, where $\Delta_1\langle B\rangle = c_{\alpha\beta}\gamma_{\alpha\beta}$, in which the coefficients $c_{\alpha\beta}$ are independent of (γ_{ij}).

Regarding the other hypotheses, i.e. the first and third hypotheses (i) and (iii) of similarity for TSF proposed in § 2.1, we assume here them to be still applicable (but the symbol c in the third hypothesis (iii) is to be understood appropriately.) When applied to $B = g_{ij}g_{mn}$, the modified hypothesis (m-ii) implies that $\Delta\langle g_{ij}g_{mn}\rangle \approx \Delta_1\langle g_{ij}g_{mn}\rangle$, where $\Delta_1\langle g_{ij}g_{mn}\rangle = c_{1,ijmn\alpha\beta}\gamma_{\alpha\beta}$, in which the coefficients $c_{1,ijmn\alpha\beta}$ are independent of (γ_{ij}). The third hypothesis (iii) then implies that $c_{1,ijmn\alpha\beta}$ must be an isotropic 6th-order tensor uniquely determined by ν and $\langle\epsilon\rangle$.

However, a simple consideration suggests that the applicability of the modified hypothesis (m-ii) under the first and third hypotheses (i) and (iii) is questionable. To see this, note that the modified hypothesis (m-ii) and the hypotheses (i) and (iii) yield an expression for $\langle g_{11}g_{11}\rangle$ like (2.35) but with $\gamma C_{1,1111}$ replaced by $\gamma_{\alpha\beta}C_{1,1111\alpha\beta}$, where $(C_{1,ijmn\alpha\beta})$ is an isotropic 6th-order tensor independent of $(\partial U_i/\partial x_j)$.

Then consider, for example, $\Delta_1\langle B\rangle$ for $B = g_{11}g_{11}$ in TCF in which $(\partial U_i/\partial x_j)$ is given by $\partial U_i/\partial x_j = \delta_{i1}\delta_{j2}[\mathrm{d}U(y)/\mathrm{d}y]$. The use of (4.9) then gives

$$\gamma_{\alpha\beta}C_{1,1111\alpha\beta} \propto C_{1,111112}\frac{\mathrm{d}U(y)}{\mathrm{d}y}, \tag{4.10}$$

while from the symmetry condition it is clear that $\langle g_{11}g_{11}\rangle$ should not depend on the sign of $\mathrm{d}U/\mathrm{d}y$. If the hypotheses (m-ii) and (iii) are to be compatible with this, (m-ii) and (iii) yield $\Delta_1\langle g_{ij}g_{mn}\rangle = 0$. Then, the hypotheses (m-ii), (i) and (iii) yield $(\nu/\langle\epsilon\rangle)\langle g_{11}g_{11}\rangle - 1/15 = o(\gamma)$ instead of (2.35). However, this appears to conflict with figure 5(*b*), which suggests $(\nu/\langle\epsilon\rangle)\langle g_{11}g_{11}\rangle - 1/15 \propto \gamma$. Thus, in view of figure 5(*b*) the applicability of the modified hypothesis (m-ii) under the first and third hypotheses (i) and (iii) is questionable.

To get some idea on the reason why $\Delta_1\langle g_{ij}g_{mn}\cdots\rangle$ needs not be linear in the disturbance parameter γ_{ij}, it is instructive to consider the fundamental solution $\boldsymbol{v}(\boldsymbol{r})$ of the so-called Oseen equation that satisfies

$$(\boldsymbol{U}\cdot\boldsymbol{\nabla})\boldsymbol{v} + \frac{1}{\rho}\boldsymbol{\nabla}p - \nu\nabla^2\boldsymbol{v} = \boldsymbol{f}\delta(\boldsymbol{r}), \quad \boldsymbol{\nabla}\cdot\boldsymbol{v} = 0, \tag{4.11}$$

and the boundary conditions

$$\boldsymbol{v} \to 0, \quad p - p_0 \to 0, \quad \text{at } r \to \infty, \tag{4.12}$$

where $\boldsymbol{U}$ and $\boldsymbol{f}$ are constant vectors, $\delta(\boldsymbol{r})$ is the three-dimensional Dirac delta function, and p_0 is a constant. The Oseen equation is similar to (2.7) in the sense that both of them include parameters representing the small disturbance [$\boldsymbol{U}$ in the Oseen equation (4.11), and $(\partial U_i/\partial x_j)$ in (2.7) with (2.8)], as small coefficients coupled to the gradient operator $\boldsymbol{\nabla}$ that works on $\boldsymbol{v}$.

Because of the linearity of (4.11), $\boldsymbol{v}$ may be written without loss of generality in the form

$$v_i(\boldsymbol{r}) = D_{i\alpha}(\boldsymbol{r})f_\alpha, \tag{4.13}$$

where the tensor $(D_{i\alpha}(\boldsymbol{r}))$ depends only on $\boldsymbol{U}$, ν and $\boldsymbol{r}$.

Suppose that we do not know how to theoretically derive the tensor (D_{ij}) for small but finite $\gamma \equiv Ur/\nu$ from the Oseen equation (4.11). Then, it is natural to assume, similarly to the first hypothesis of similarity for TSF, the following hypothesis.

(i′) The first hypothesis of similarity for D_{ij}.
In the limit $\gamma \to 0$, (D_{ij}) is an isotropic tensor and is uniquely determined by ν and $\boldsymbol{r}$ independently of $\boldsymbol{U}$.

From this assumption, one can correctly arrive at

$$D_{ij}(\boldsymbol{r}) \to D_{e,ij}(\boldsymbol{r}) = \frac{1}{\nu r}F_{ij}(\hat{\boldsymbol{r}}), \tag{4.14}$$

at $\gamma \to 0$, where $(F_{ij}(\hat{\boldsymbol{r}}))$ is an isotropic second-order tensor that depends on only $\hat{\boldsymbol{r}} \equiv \boldsymbol{r}/r$ and is independent of $\boldsymbol{U}$ and ν.

For small but finite γ, let $D_{ij}(\boldsymbol{r})$ be written as

$$D_{ij}(\boldsymbol{r}) = D_{e,ij}(\boldsymbol{r}) + \Delta D_{ij}(\boldsymbol{r}). \tag{4.15}$$

Then, one might assume the following two hypotheses:

(ii′) The second hypothesis of similarity for D_{ij}.
For sufficiently small but finite γ, the change ΔD_{ij} of D_{ij} owing to the finite vector $(\gamma_i) \equiv (U_i r/\nu)$ can be approximated to be linear in (γ_i), i.e. $\Delta D_{ij} \approx \Delta_1 D_{ij}$, where $\Delta_1 D_{ij} = c_{ij\alpha}\gamma_\alpha = c_{ij\alpha}U_\alpha r/\nu$, in which the coefficients $c_{ij\alpha}$ are independent of (γ_i).

(iii′) The third hypothesis of similarity for D_{ij}.
The tensor $(c_{ij\alpha})$ is an isotropic third-order tensor that is uniquely determined by ν and $\boldsymbol{r}$.

The second and third hypotheses give

$$\Delta D_{ij}(\boldsymbol{r}) = \frac{1}{\nu r}\left[C_{ij\alpha}(\hat{\boldsymbol{r}})\frac{U_\alpha r}{\nu} + o(\gamma)\right], \tag{4.16}$$

where $C_{ij\alpha}(\hat{\boldsymbol{r}})$ are functions only of $\hat{\boldsymbol{r}} = \boldsymbol{r}/r$, and satisfy $C_{ij\alpha}(-\hat{\boldsymbol{r}}) = -C_{ij\alpha}(\hat{\boldsymbol{r}})$. This implies that the leading-order terms $\Delta_1 D_{ij}(\boldsymbol{r})$ of $\Delta D_{ij}(\boldsymbol{r})$ for small Ur/ν satisfy $\Delta_1 D_{ij}(-\boldsymbol{r}) = -\Delta_1 D_{ij}(\boldsymbol{r})$.

However, this is in conflict with the exact solution of the Oseen equation (4.11) (readers may refer to standard textbooks in fluid mechanics regarding this point). Thus, this example suggests that the response $\Delta\langle B\rangle$ is not necessarily linear in the vector or the tensor representing the disturbance [$\boldsymbol{U}$ in (4.11), $(\partial U_i/\partial x_j)$ in (2.7) with (2.8)], provided that the coefficients, such as $c_{ij\alpha}$ and $c_{1,ijmn\alpha\beta}$, must satisfy certain conditions, such as the isotropy condition.

The above discussions do not exclude the possibility that the modified hypothesis (m-ii) and the first and third hypotheses (i) and (ii) hold and some DNS results unaccountable by them are due to (an) unidentified effect(s) other than that of mean shear gradients.

4.3. *Conclusions*

In this study, we proposed an extension of the idea of K41 to take into account the influence of the mean shear in TSF on the statistics in the DR. In the extension, we introduced three hypotheses for the small-scale statistics in TSF;

(i) (the first hypothesis) local isotropy in the limit $\gamma \to 0$,
(ii) (the second hypothesis) approximate linearity of $\Delta\langle B\rangle$ in γ, i.e. $\Delta\langle B\rangle \approx \Delta_1\langle B\rangle = c\gamma$, for sufficiently small but finite γ,
(iii) (the third hypothesis) localness of the coefficient c in the expression $\Delta_1\langle B\rangle = c\gamma$,

where γ is a local dimensionless measure of the strength of the mean shear, $\Delta\langle B\rangle$ is the change of the average of the observable B due to the mean shear and $\Delta_1\langle B\rangle$ is the leading-order term of $\Delta\langle B\rangle$ for small γ.

When applied to the second-order moments of the gradients g_{ij} of the fluctuating velocity field in the inertial sublayer of wall turbulence, the extension gives estimates of the dependence of the moments of g_{ij} on the distance from the wall. Particular attention is paid to the second-order moments $\langle g_{ij}g_{kj}\rangle$ which make up the energy dissipation rate tensor $(\epsilon_{ij}) \equiv 2\nu(\langle g_{i\alpha}g_{j\alpha}\rangle)$, and the theory was tested by comparison with the data of DNSs of turbulent channel flow with friction Reynolds numbers R_τ up to approximately 8000.

The comparison shows that the hypothesis (i) is consistent with the approach of the statistics by the DNSs to the values given by the isotropy and locality assumptions with an increase in y^+ as seen in figures 5(*a*,*c*,*e*), 6, 9 and 11, and also that the hypotheses (ii) and

(iii) are consistent with the slopes by the DNSs observed in figures 5(*b*,*d*,*f*), 7, 8, 10 and 12. These results suggest that the simple hypotheses are in reasonable agreement with the DNSs.

Funding. This work was partly supported by JSPS KAKENHI Grant Numbers JP16H06339, JP19H00641 and JP18K03923. The data analysis used computational resources of NEC SX-ACE provided by Japan Agency for Marin-Earth Science and Technology and Tohoku University through the HPCI System Research project (Project IDs: hp190108 and hp20107).

Declaration of interests. The authors report no conflict of interest.

Author ORCIDs.
Yukio Kaneda https://orcid.org/0000-0001-7963-0985;
Yoshinobu Yamamoto https://orcid.org/0000-0002-6082-1391.

Appendix A. Turbulent kinetic energy and energy dissipation rate budget terms in turbulent channel flow

We assume here that the mean flow $\boldsymbol{U}$ is given by $\boldsymbol{U} = (U_1, 0, 0)$ and the statistics are homogeneous in the x_1- and x_3-directions, and use the notation in Mansour *et al.* (1988) (but in a dimensional form and a typo is corrected).

The equation for the mean turbulent kinetic energy $k = \langle u_\alpha u_\alpha \rangle /2$ can be then written as

$$\frac{\mathrm{D}k}{\mathrm{D}t} = P_k + T_k + \Pi_k + D_k - \langle \epsilon \rangle \,, \tag{A1}$$

where $\mathrm{D}/\mathrm{D}t \equiv \partial/\partial t + U_1 \partial/\partial x_1$, and the budget terms on the right-hand side are given by

$$P_k = -\langle u_1 u_2 \rangle \frac{\partial U_1}{\partial x_2}, \tag{A2}$$

$$T_k = \frac{-1}{2} \frac{\partial}{\partial x_2} \left(\langle u_1 u_1 u_2 \rangle + \langle u_2 u_2 u_2 \rangle + \langle u_3 u_3 u_2 \rangle \right), \tag{A3}$$

$$\Pi_k = -\frac{\partial}{\partial x_2} \left\langle \frac{p u_2}{\rho} \right\rangle, \tag{A4}$$

$$D_k = \nu \frac{\partial^2 k}{\partial x_2^2}, \tag{A5}$$

$$\langle \epsilon \rangle = \nu \left\langle \frac{\partial u_\alpha}{\partial x_\beta} \frac{\partial u_\alpha}{\partial x_\beta} \right\rangle. \tag{A6}$$

The equation for mean energy dissipation rate $\langle \epsilon \rangle$ can be written as

$$\frac{\mathrm{D}\langle \epsilon \rangle}{\mathrm{D}t} = P_\epsilon^1 + P_\epsilon^2 + P_\epsilon^3 + P_\epsilon^4 + T_\epsilon + \Pi_\epsilon + D_\epsilon - \gamma_\epsilon, \tag{A7}$$

where the $\langle \epsilon \rangle$-budget terms on the right-hand side are given by

$$P_\epsilon^1 = -2\nu \left\langle \frac{\partial u_1}{\partial x_\alpha} \frac{\partial u_2}{\partial x_\alpha} \right\rangle \frac{\partial U_1}{\partial x_2}, \tag{A8}$$

$$P_\epsilon^2 = -2\nu \left\langle \frac{\partial u_\alpha}{\partial x_1} \frac{\partial u_\alpha}{\partial x_2} \right\rangle \frac{\partial U_1}{\partial x_2}, \tag{A9}$$

$$P_\epsilon^3 = -2\nu \left\langle u_2 \frac{\partial u_1}{\partial x_2} \right\rangle \frac{\partial^2 U_1}{\partial x_2^2}, \tag{A10}$$

$$P_\epsilon^4 = -2\nu \left\langle \frac{\partial u_\alpha}{\partial x_\beta} \frac{\partial u_\alpha}{\partial x_\gamma} \frac{\partial u_\gamma}{\partial x_\beta} \right\rangle, \tag{A11}$$

$$T_\epsilon = -\nu \frac{\partial}{\partial x_2} \left\langle \frac{\partial u_\alpha}{\partial x_\beta} \frac{\partial u_\alpha}{\partial x_\beta} u_2 \right\rangle, \tag{A12}$$

$$\Pi_\epsilon = -2\nu \frac{\partial}{\partial x_2} \left\langle \frac{1}{\rho} \frac{\partial p}{\partial x_\alpha} \frac{\partial u_2}{\partial x_\alpha} \right\rangle, \tag{A13}$$

$$D_\epsilon = \nu \frac{\partial^2 \langle \epsilon \rangle}{\partial x_2^2}, \tag{A14}$$

$$\gamma_\epsilon = 2\nu^2 \left\langle \frac{\partial^2 u_\alpha}{\partial x_\beta \partial x_\gamma} \frac{\partial^2 u_\alpha}{\partial x_\beta \partial x_\gamma} \right\rangle. \tag{A15}$$

Appendix B. Estimates of terms on the right-hand sides of (4.3)–(4.5)

Since (2.2*b*,*c*) gives $\boldsymbol{r}_0 = \boldsymbol{x}_0$ at time $t = t_0$, i.e. $s = 0$, $\boldsymbol{V}$ and $\boldsymbol{v}^L$ can be respectively expanded for small $r \equiv |\boldsymbol{r}|$ as (2.8) and

$$\boldsymbol{v}^L = \boldsymbol{u}^L(\boldsymbol{r} + \boldsymbol{x}_0) - \boldsymbol{u}^L(\boldsymbol{x}_0) = \frac{\partial \boldsymbol{u}^L}{\partial x_\alpha} r_\alpha + \cdots, \tag{B1}$$

at $s = 0$, where $\partial \boldsymbol{u}^L / \partial x_\alpha = \partial \boldsymbol{u}^L / \partial x_\alpha |_{x=x_0}$. In view of (2.8) and (B1), rough order estimates of the terms in (4.3), (4.4) and (4.5) for $r \sim \eta$ are obtained by using

$$\boldsymbol{V} \sim S\eta, \quad \boldsymbol{v}^L \sim \frac{\partial \boldsymbol{u}^L}{\partial x_\alpha} \eta \sim \frac{u'}{\ell} \eta, \quad \boldsymbol{v}^S \sim v_\eta, \tag{B2a–c}$$

and

$$(\nabla \boldsymbol{V}, \nabla \boldsymbol{v}^L, \nabla \boldsymbol{v}^S) \sim \frac{1}{\eta} (\boldsymbol{V}, \boldsymbol{v}^L, \boldsymbol{v}^S), \tag{B3}$$

where $3(u')^2 = \langle \boldsymbol{u} \cdot \boldsymbol{u} \rangle$, and ℓ is the characteristic length scale of large-scale energy-containing eddies. Equations (B2) and (B3) give

$$\boldsymbol{V} \sim \gamma \boldsymbol{v}^S, \quad \boldsymbol{v}^L \sim \gamma_e \boldsymbol{v}^S, \tag{B4a,b}$$

and

$$\nabla \boldsymbol{V} \sim \gamma \nabla \boldsymbol{v}^S, \quad \nabla \boldsymbol{v}^L \sim \gamma_e \nabla \boldsymbol{v}^S, \tag{B5a,b}$$

where γ_e is given by (4.7). We therefore have

$$(\boldsymbol{v}^S \cdot \nabla) \boldsymbol{v}^S \sim \frac{v_\eta^2}{\eta}, \tag{B6}$$

$$(\boldsymbol{V} \cdot \nabla) \boldsymbol{v}^L \sim (\boldsymbol{v}^L \cdot \nabla) \boldsymbol{V} \sim \gamma \gamma_e \frac{v_\eta^2}{\eta}, \tag{B7}$$

$$(\boldsymbol{V}\cdot\boldsymbol{\nabla})\boldsymbol{v}^S \sim (\boldsymbol{v}^S\cdot\boldsymbol{\nabla})\boldsymbol{V} \sim \gamma\frac{v_\eta^2}{\eta}, \tag{B8}$$

$$(\boldsymbol{v}^L\cdot\boldsymbol{\nabla})\boldsymbol{v}^L \sim \gamma_e^2\frac{v_\eta^2}{\eta}, \tag{B9}$$

and

$$(\boldsymbol{v}^L\cdot\boldsymbol{\nabla})\boldsymbol{v}^S \sim (\boldsymbol{v}^S\cdot\boldsymbol{\nabla})\boldsymbol{v}^L \sim \gamma_e\frac{v_\eta^2}{\eta}. \tag{B10}$$

References

Abe, H. & Antonia, R.A. 2016 Relationship between the energy dissipation function and the skin friction law in a turbulent channel flow. *J. Fluid Mech.* **798**, 140–164.

Antonia, R.A., Djenidi, L. & Spalart, P.R. 1994 Anisotropy of the dissipation tensor in a turbulent boundary layer. *Phys. Fluids* **6** (7), 2475–2479.

Antonia, R.A., Kim, J. & Browne, L.W.B. 1991 Some characteristics of small-scale turbulence in a turbulent duct flow. *J. Fluid Mech.* **233**, 369–388.

Bernardini, M., Pirozzoli, S. & Orlandi, P. 2014 Velocity statistics in turbulent channel flow up to $Re_\tau = 4000$. *J. Fluid Mech.* **742**, 171–191.

Bolotnov, I.A., Lahey, R.T., Jr., Drew, D.A., Jansen, K.E. & Oberai, A.A. 2010 Spectral analysis of turbulence based on the DNS of a channel flow. *Comput. Fluids* **39**, 640–655.

Bradshaw, P. & Perot, J.B. 1993 A note on turbulent energy dissipation in the viscous wall region. *Phys. Fluids* **5** (12), 3305–3306.

Browne, L.W.B., Antonia, R.A. & Shah, D.A. 1987 Turbulent energy dissipation in a wake. *J. Fluid Mech.* **179**, 307–326.

Cambon, C. & Rubinstein, R. 2006 Anisotropic developments for homogeneous shear flows. *Phys. Fluids* **18** (8), 085106.

Chin, C., Philip, J., Klewicki, J., Ooi, A. & Marusic, I. 2014 Reynolds-number-dependent turbulent inertia and onset of log region in pipe flows. *J. Fluid Mech.* **757**, 747–388.

Corrsin, S. 1958 Local isotropy in turbulent shear flow. *N.A.C.A. Res. Memo.* RM 58B11.

Folz, A. & Wallace, J.M. 2010 Near-surface turbulence in the atmospheric boundary layer. *Physica* D **239** (14), 1305–1317.

George, W. & Hussein, H.J. 1991 Locally axisymmetric turbulence. *J. Fluid Mech.* **233**, 1–23.

Hinze, J.O. 1975 *Turbulence*, 2nd edn. McGraw-Hill.

Honkan, A. & Andreopoulos, Y. 1997 Vorticity, strain-rate and dissipation characteristics in the near-wall region of turbulent boundary layers. *J. Fluid Mech.* **350**, 29–96.

Hoyas, S. & Jiménez, J. 2006 Scaling of the velocity fluctuations in turbulent channels up to $Re_\tau = 2003$. *Phys. Fluids* **18** (1), 011702.

Ishihara, T., Yoshida, K. & Kaneda, Y. 2002 Anisotropic velocity correlation spectrum at small scales in a homogeneous turbulent shear flow. *Phys. Rev. Lett.* **88**, 154501.

Jiménez, J. & Moser, R.D. 2007 What are we learning from simulating wall turbulence? *Phil. Trans. R. Soc. Lond.* A **365**, 715–732.

Kaneda, Y. 2020 Linear response theory of turbulence. *J. Stat. Mech.* **2020**, 034006.

Kaneda, Y., Morishita, K. & Ishihara, T. 2013 Small scale universality and spectral characteristics in turbulent flow. In *Proc. Eighth International Symposium on Turbulence and Shear Flow Phenomena*, Begel House.

Kaneda, Y. & Yoshida, K. 2004 Small-scale anisotropy in stably stratified turbulence. *New J. Phys.* **6**, 34.

Kida, S. & Orszag, S.A. 1990 Energy and spectral dynamics in forced compressible turbulence. *J. Sci. Comput.* **5**, 85–125.

Klewicki, J.C. 2010 Reynolds number dependence, scaling, and dynamics of turbulent boundary layers. *Trans. ASME J. Fluids Engng* **132**, 094001.

Kolmogorov, A.N. 1941 The local structure of turbulence in incompressible viscous fluid for very large Reynolds numbers. *C. R. Acad. Sci. USSR* **30**, 301–305.

Livescu, D. & Madnia, C.K. 2004 Small scale structure of homogeneous turbulent shear flow. *Phys. Fluids* **16** (8), 2864–2876.

LEE, M. & MOSER, R.D. 2015 Direct numerical simulation of turbulent channel flow up to $Re_\tau \approx 5200$. *J. Fluid Mech.* **774**, 395–415.

LEE, M. & MOSER, R.D. 2019 Spectral analysis of the budget equation in turbulent channel flows at high Reynolds number. *J. Fluid Mech.* **860**, 886–938.

LESLIE, D.C. 1973 *Developments in the Theory of Turbulence*. Clarendon Press.

LOUCKS, R.B. & WALLACE, J.M. 2012 Velocity and velocity gradient based properties of a turbulent plane mixing layer. *J. Fluid Mech.* **699**, 280–319.

LUMLEY, J.L. 1967 Similarity and the turbulent energy spectrum. *Phys. Fluids* **10** (4), 855–858.

MANSOUR, N.N., KIM, J. & MOIN, P. 1988 Reynolds-stress and dissipation-rate budgets in a turbulent channel flow. *J. Fluid Mech.* **194**, 15–44.

MENEVEAU, C. 2011 Lagrangian dynamics and models of the velocity gradient tensor in turbulent flows. *Annu. Rev. Fluid Mech.* **43**, 219–245.

MORISHITA, K., ISHIHARA, T. & KANEDA, Y. 2019 Length scales in turbulent channel flow. *J. Phys. Soc. Japan* **88**, 064401.

PUMIR, A., XU, H. & SIGGIA, E.D. 2016 Small-scale anisotropy in turbulent boundary layers. *J. Fluid Mech.* **804**, 5–23.

PUMIR, A. 2017 Structure of the velocity gradient tensor in turbulent shear flows. *Phys. Rev. Fluids* **2**, 074602.

SADDOUGHI, S.G. & VEERAVALLI, S.V. 1994 Local isotropy in turbulent boundary layers at high Reynolds number. *J. Fluid Mech.* **268**, 333–372.

SAGAUT, P. & CAMBON, C. 2018 *Homogeneous Turbulence Dynamics*. 2nd edn. Springer.

SCHUMACHER, J., SREENIVASAN, K.R. & YEUNG, P.K. 2003 Derivative moments in turbulent shear flows. *Phys. Fluids* **15** (1), 84–90.

TARDU, S. 2017 Near wall dissipation revisited. *Intl J. Heat Fluid Flow* **67**, 104–115.

TSINOBER, A., KIT, E. & DRACOS, T. 1992 Experimental investigation of the field of velocity gradients in turbulent flows. *J. Fluid Mech.* **242**, 169–192.

TENNEKES, H. & LUMLEY, J.L. 1972 *A First Course in Turbulence*. The MIT Press.

TSUJI, Y. & KANEDA, Y. 2012 Anisotropic pressure correlation spectra in turbulent shear flow. *J. Fluid Mech.* **694**, 50–77.

VREMAN, A.W. & KUERTEN, J.G.M. 2014 Statistics of spatial derivatives of velocity and pressure in turbulent channel flow. *Phys. Fluids* **26** (8), 085103.

YAMAMOTO, Y. & KUNUGI, T. 2011 Direct numerical simulation of a high-Froude-number turbulent open-channel flow. *Phys. Fluids* **23** (12), 125108.

YAMAMOTO, Y. & KUNUGI, T. 2016 MHD effects on turbulent dissipation process in channel flows with an imposed wall-normal magnetic field. *Fusion Engng Des.* **109**, 1137–1142.

YAMAMOTO, Y. & TSUJI, Y. 2018 Numerical evidence of logarithmic regions in channel flow at $Re_\tau = 8000$. *Phys. Rev. Fluids* **3**, 012602.

YOSHIDA, K., ISHIHARA, T. & KANEDA, Y. 2003 Anisotropic spectrum of homogeneous turbulent shear flow in a Lagrangian renormalized approximation. *Phys. Fluids* **15** (8), 2385–2397.

YOSHIZAWA, A. 1998 *Hydrodynamic and Magnetohydrodynamic Turbulent Flows*. Kluwer Academic.